Origin of Solid-State Activated Sintering in Bi_2O_3-Doped ZnO

by

Jian Luo

Bachelor of Engineering, Materials Science and Engineering
Bachelor of Engineering (Minor), Electronics and Computer Technology
Tsinghua University, Beijing, China (1994)

Submitted to the Department of Materials Science and Engineering
in Partial Fulfillment of the Requirements for the Degree of

Master of Science in Materials Science and Engineering

at the
Massachusetts Institute of Technology
June 1999

Signature of Author.....
Department of Materials Science and Engineering
May 7, 1999

Certified by.....
Professor Yet-Ming Chiang
Kyocera Professor of Ceramics
Thesis Supervisor

Accepted by.....
Professor Linn W. Hobbs
John F. Elliott Professor of Materials
Chairman, Departmental Committee on Graduate Students

Origin of Solid-State Activated Sintering in Bi_2O_3-Doped ZnO

by

Jian Luo

Submitted to the Department of Materials Science and Engineering on May 7, 1999
in Partial Fulfillment of the Requirements for the Degree of
Master of Science in Materials Science and Engineering

ABSTRACT

Activated sintering in Bi_2O_3-doped ZnO has been studied with emphasis on the mechanistic role of intergranular amorphous films. The atomic-level microstructures and bismuth solute distributions in doped powders have been investigated using high resolution electron microscopy (HREM) and scanning transmission electron microscopy (STEM). Densification is observed to be significant below the bulk eutectic temperature in the presence of Bi_2O_3 concentrations as low as 0.58 mole %. Transmission electron microscopy (TEM) of as-calcined and sintered powders shows that significant neck growth and particle coarsening occur in the solid state. Intergranular amorphous films of ~1 nm thickness, terminating in wetting menisci at sinter-necks, are observed to form concurrently with the onset of activated sintering. In a few instances, amorphous films are also observed at surfaces of the ZnO particles. Activated sintering in this binary system is attributed to rapid mass transport through sub-eutectic, equilibrium-thickness intergranular films, with the amorphous phase also providing capillary pressure.

Thesis Supervisor: Professor Yet-Ming Chiang
Title: Kyocera Professor of Ceramics

Table of Contents

List of Illustrations and Figures

List of Table

Acknowledgments

First, I would like to thank my advisor Professor Yet-Ming Chiang for providing me the chance to do graduate research at MIT, for all his helpful insights, and for providing a good balance of guidance and freedom.

I am thankful to all my group members who helped me with my research. Dr. H. Wang, contributed this work by taking the HREM pictures (Figure 7, 10 and 13). I acknowledge Dr. J. -R. Lee for providing the powders used in this work and A. Soukojak for his help in dilatometry. D. A. Blom, Y. –I. Jang, H. Ackler and E. B. Erin helped me in many aspects when I first joined the group.

Thanks to Dr. A. J. Garratt-Reed, Mr. M. Frongillo and Dr. D. C. Bell for assistance and training with TEM and STEM, and Mr. Joe Adario for help with X-ray diffraction experiments. Ms. Toni Centorino and Mr. Fred Wilson provide a stable support during my research.

Finally, I would like to thank my parents for good instruction early on and for supporting me all the time.

1. Introduction

1.1. Activated Sintering

Activated sintering refers to the phenomenon whereby sintering rates are improved due to solid-state additives, and has generally been attributed to the presence of a secondary or "activator" phase. Because previous research has shown that densification and neck growth occur at temperature where lattice diffusion is too slow to contribute significantly to the shrinkage, grain boundary or surface transport is usually implicated. Nickel-doped tungsten has been widely studied as a model system for activated sintering, and a quantitative analysis based on a liquid phase sintering model [1] has been developed [2]. In this model, when each tungsten particle is first coated with a uniform nickel layer, the nickel phase is presumed to provide a short-circuit diffusion path for mass transport of tungsten (Figure 1). Activated sintering has been reported in various metallic [3, 4] and ceramic systems [5-7], and similar physical models have been assumed for over 30 years [8-10].

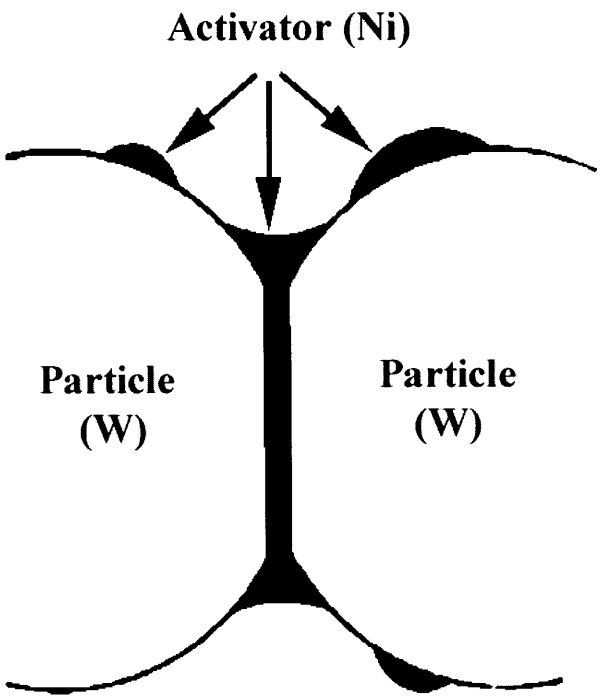

Figure 1 A schematic illustration of nickel activated sintering of tungsten.

When a deliberate coating is not applied, the enhancement of mass transport is generally attributed to a secondary phase that completely or partially wets the primary phase and penetrates along grain boundaries [11]. In general it is also possible that segregation of additives without the formation of a discrete secondary phase can enhance diffusion. Because the effective coating thickness in activated sintering of tungsten is only a few monolayers [8, 9], high resolution techniques such as HREM and STEM are necessary to investigate these layers. However, to date these presumed "activators" have not been directly observed in sufficient detail to understand their morphology, structure and chemistry.

The essential prerequisites for a solid-state activator phase are similar to those for liquid phase sintering additives; it should have high solubility for the base material, should remain segregated at grain boundaries, and should have a high transport rate for the primary phase [11, 12]. German et al. [11] suggested that activated sintering systems would likely be identified using equilibrium phase diagrams. However, this approach neglects the possibility of interfacial phases that do not exist in the bulk phase diagram.

Bismuth-doped zinc oxide is the basis for varistors that exhibit nonlinear voltage-current characteristics [13, 14]. The binary phase dirgarm is shown in Figure 2. This system has been studied as a model system for liquid-phase sintering [15]. Previous experiments [16-20] have also shown that there is enhanced sintering below the eutectic temperature (740°C). Isothermal experiments indicate that a combination of grain boundary and surface diffusion controls the solid-state sintering kinetics[16]. Rahaman et al. [17] observed pronounced shrinkage below 710°C in ZnO doped with Bi_2O_3, MnO, and CoO, and inferred an "unknown chemical reaction between the powder constituents" at about 650°C, leading to the formation of a "pre-eutectic liquid phase." A similar phenomenon was found by Ghirlanda et al. [18], who suggested a "pre-liquid-phase" effect. Peigney and Rousset [19] performed dilatometric measurements and thermal analysis on zinc oxide powders co-precipitated with bismuth, and suggested the occurrence of "transient melting" below the eutectic temperature. Kim et al. [20] also reported significant shrinkage below the eutectic temperature.

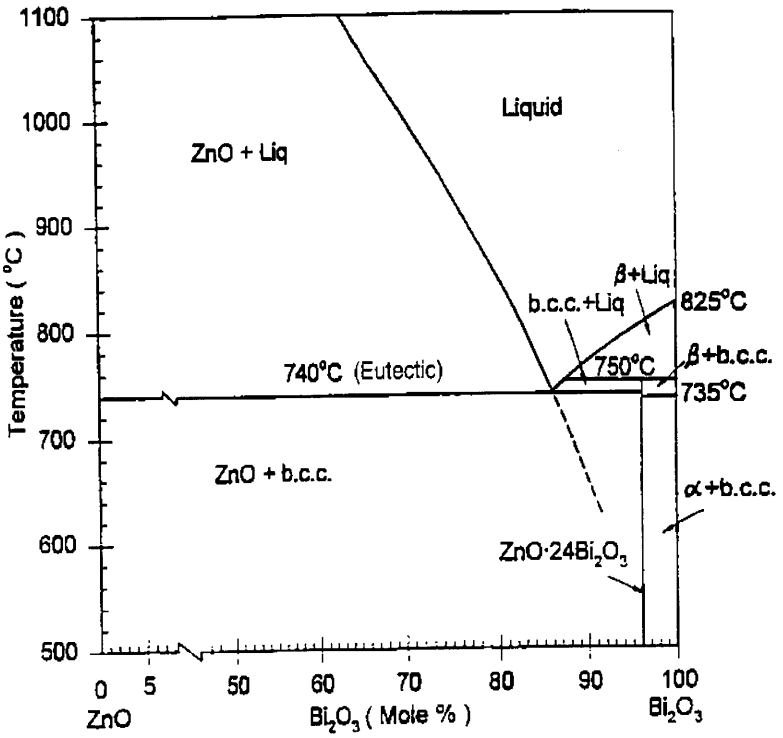

Figure 2 $ZnO - Bi_2O_3$ phase diagram [21-22].

1.2. Intergranular Films

Equilibrium-thickness intergranular films have been observed in many ceramic systems, including Si_3N_4, Al_2O_3, ZrO_2, RuO_2 and SiC doped with various additives [23-30]. The thickness of the films is on the order of one nanometer, is nearly constant along the boundary, and varies little from boundary to boundary [23-24]. Dihedral angles are nonzero where boundary films intersect glass pockets.

Clarke [23] proposed that the thickness of the intergranular films represents an equilibrium separation between grains. In the simplest form of this model, the total free energy is the sum of van der Waals attractive interaction and a steric (ordering or structural) repulsive interaction, and the film has a local minimum (at the equilibrium thickness) where the attractive and repulsive forces balance.

A generalized treatment of the ordering force has recently been presented [24]. Films have also been observed at heterophase interfaces [27, 29]. In addition amorphous films have been shown to be the equilibrium interfacial phases at TiO_2-SiO_2 hetero-phase interfaces [29], well below the solidus temperature.

The structure and chemistry of grain boundaries in ZnO varistors have been extensively investigated by various researchers [31-36]. Recently, Wang and Chiang [30] showed that intergranular amorphous films of ~1 nm thickness form at equilibrium below the eutectic temperature (Figure 3). These films possess a ZnO-rich composition that is distinct from the eutectic liquid or any intermediate compounds in this binary system [21-22]. Moreover, the grain boundary oxygen diffusion coefficient in samples containing the intergranular amorphous films has been found to be 10^5-10^6 higher than that in undoped samples [37]. These facts suggested to us that the intergranular amorphous films would likely be responsible for activated sintering in Bi_2O_3-doped ZnO ceramics.

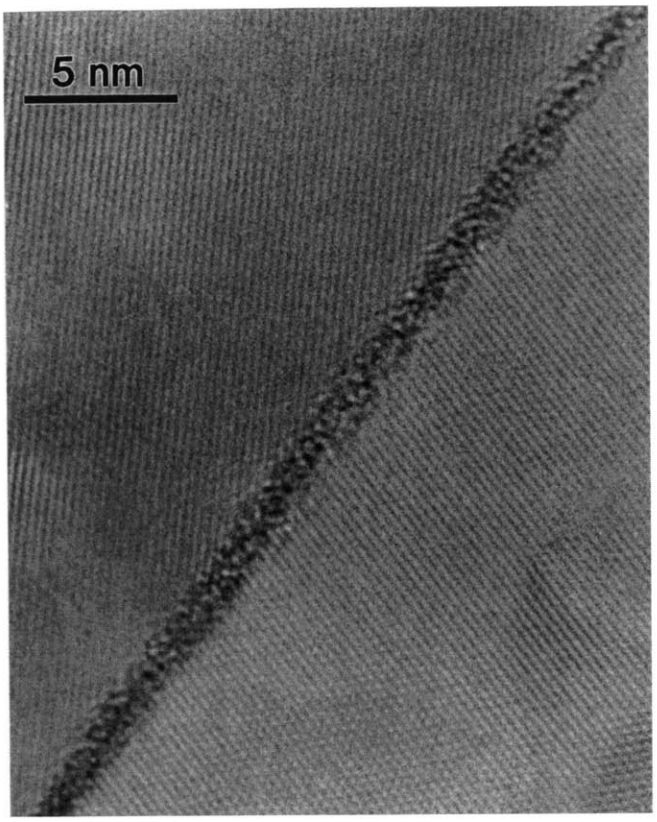

Figure 3 An amorphous intergranular film formed below the bulk eutectic temperature. Courtesy of H. Wang (H. Wang and Y.-M. Chiang, *J. Am. Ceram. Soc.* **81** [1], 89-96 (1998)).

2. Experimental

Bismuth-doped zinc oxide powders were prepared by a co-precipitation method that has been described elsewhere [33]. The precipitated powders were calcined in air at 500°C for 2 hours, and the calcined powders (without any organic binder) were cold-pressed into pellets (6.2 mm diameter, 2~3 mm thickness) at about 20-25 MPa. The green density is around 60%, 55%, 40%, and 30%, respectively, for ZnO doped with 0% (pure ZnO), 0.23%, 0.58%, and 6.5% Bi_2O_3 respectively. Shrinkage curves were measured using an automatic recording dilatometer (Orton, Westville, OH). The

temperature was increased at 5°C/min to 550°C, then the dilatometric measurements were performed from that point forth at heating rates of 2°C/min, 0.5°C/min and 0.067°C/min (4°C/hour) respectively. The linear thermal expansion was subtracted from the shrinkage curves.

TEM specimens are difficult to prepare from lightly sintered pellets. In addition to difficulties in sectioning, the ion-thinning process can introduce artifacts [30]. Therefore, we prepared samples from uncompacted powders and subjected them to the same heat treatment as the sintered samples. Calcined powders were wrapped in platinum foil and heated in a programmable furnace at 4°C/hour to 650°C or 700°C, and air-quenched. TEM specimens were then prepared by dispersing the powders ultrasonically in acetone and dropping a small amount of the suspension onto carbon-coated copper grids. A JEOL JEM-200CX electron microscope was used to observe the as-calcined and sintered powders at low magnifications. High resolution electron microscopy was then carried out on a Topcon/Akashi EM-002B microscope operating at 200kV with a ±10° double-tilt sample holder. The bismuth and zinc distributions were mapped using a Fisons / Vacuum Generators HB603 analytical STEM equipped with a Link Systems energy dispersive X-ray (EDX) analyzer. X-ray diffraction (XRD, Rigaku, RU 300 X-ray generator, Cu Kα radiation) were conducted on sintered powders.

Particle size statistics of as-calcined and sintered powders were also collected. The diameter of clearly separated particles was measured at a magnification of 50,000×. The square root of the product of the long and short axial diameters was used for

particles of elliptical cross-section. An equivalent diameter corresponding to the same projected area was used for irregularly shaped particles.

Ultrasonically dispersed powder specimens were prepared, and a set of TEM samples was prepared by placing the dry powders directly on copper grids. These two types of specimens gave results that were consistent with one another. The final statistics included both sets of samples, and in all cases, more than 100 particles per sample were counted.

3. Results

3.1 Dilatometric Measurements of Pre-Eutectic Densification

Figure 4 (a)-(c) shows the shrinkage versus temperature for ZnO powder doped with 0.58 mole % Bi_2O_3 and sintered at 2°C/min, 0.5°C/min, and 0.067°C/min (4°C/hour) respectively. Sintering begins well below the eutectic temperature, and accelerates at about 700°C at the doping level of 0.58 mole % Bi_2O_3. The total shrinkage is 2%, 3.5%, and 16% for the three heating rates, respectively, at the eutectic temperature (740°C). A pure zinc oxide green pellet prepared by the same method was sintered under the lowest heating rate of 4°C/hour as a reference (Figure 4(d)). It exhibited no detectable shrinkage under these conditions.

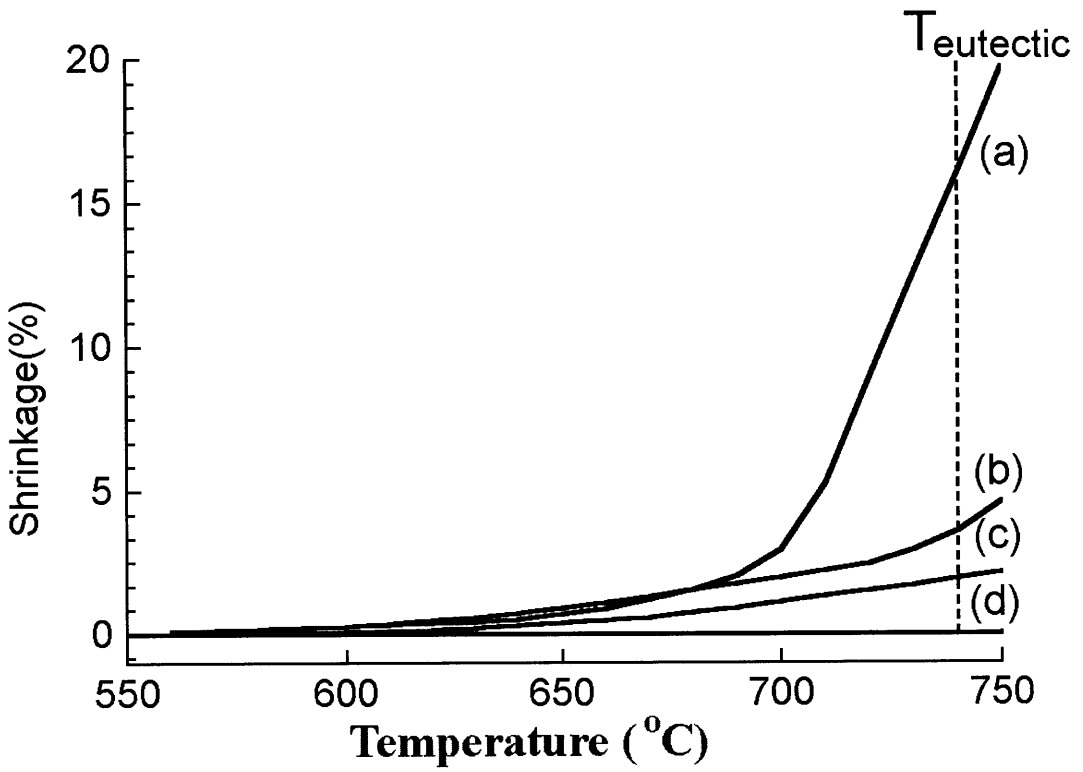

Figure 4 Shrinkage versus temperature for ZnO + 0.58 mole % Bi_2O_3 at heating rates of (a) 4°C/hour, (b) 0.5°C/minute and (c) 2°C/minute, and for (d) pure ZnO at the heating rate of 4°C/hour.

No obvious pre-eutectic densification was observed at a lower Bi_2O_3 concentration of 0.23 mole %. Pre-eutectic densification was also observed at a higher concentration of 6.5 mole % Bi_2O_3. This high bismuth content sample showed greater shrinkage below 650°C at the same heating rate of 4°C/hour, as shown on an expanded scale in Figure 5. However, the total shrinkage upon reaching the eutectic temperature is somewhat lower, at 7.25%.

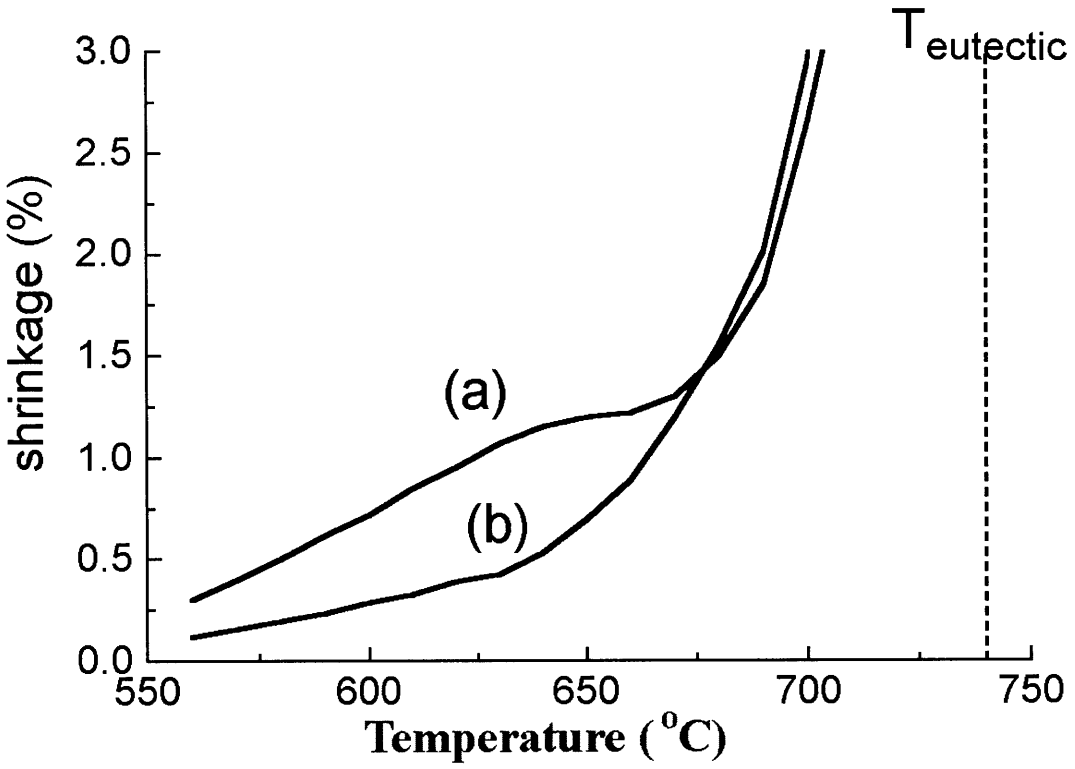

Figure 5 Shrinkage versus temperature for (a) ZnO + 6.5 mole % Bi_2O_3, and (b) ZnO + 0.58 mole % Bi_2O_3 at the heating rate of 4°C/hour.

3.2 Phase Characterization, Morphology and Size Distribution of As-Calcined and Sintered Powders

The minor phase can not be determined unequivocally by X-ray diffraction at the low doping levels used. From the few reflections observable in the sintered powder (heated at 4°C/h and quenched from 700°C), a crystalline Bi-rich phase does appear to be present, and is either the equilibrium $ZnBi_{38}O_{60}$ phase (An earlier report of this compound as $ZnBi_{48}O_{73}$ [21] has since been corrected [22].) or a metastable β phase of Bi_2O_3 [38].

In the as-calcined powder, bismuth-enriched oxide is uniformly dispersed as nanometer-sized clusters on the surfaces of the ZnO particles. Figure 6 (a) and (b) are the STEM dark field image and bismuth map of the as-calcined ZnO-0.58 mole % Bi_2O_3 powder. In the dark field image, the spots on the surfaces of ZnO particles are found in the bismuth map to correspond with bismuth-rich regions. A HREM micrograph of the bismuth oxide clusters is illustrated in Figure 7. These clusters are crystalline; although the lattice fringes are not clear in Figure 7 because of vibration during photography, they can be viewed clearly *in-situ* using the TV imaging mode of the microscope.

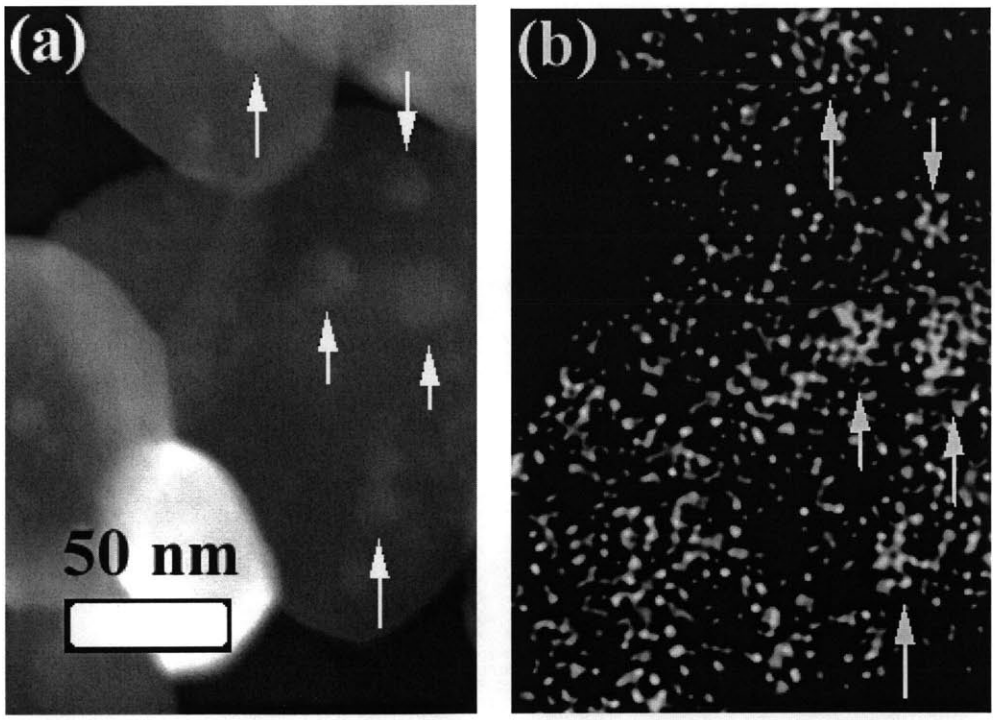

Figure 6 STEM (a) dark field image and (b) bismuth map of as-calcined ZnO + 0.58 mole % Bi_2O_3 powder. The bismuth-enriched clusters are visible as bright spots.

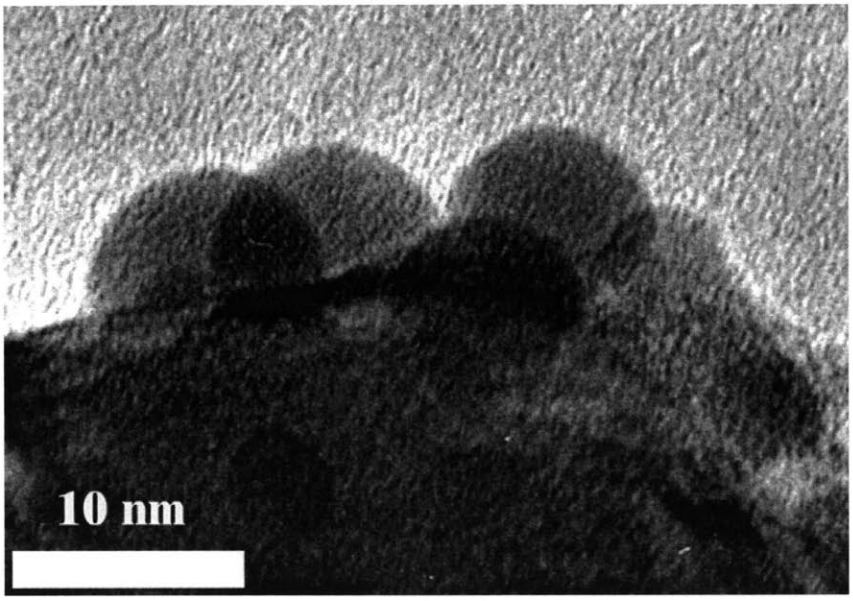

Figure 7 HREM image of bismuth-enriched nano-crystals in as-calcined ZnO + 0.58 mole % Bi_2O_3 powder.

The morphologies of as-calcined and sintered powders are shown in Figure 8 and Figure 9. We directed our attention to the ZnO powder doped with 0.58 mole % Bi_2O_3, and heated at 4°C/hour, because this composition and heating rate clearly showed activated sintering without having a large excess of secondary phase. As-calcined particles are equiaxed, relatively uniform in size, and exhibit some aggregation (Figure 8). Classical sintered powder morphologies with extensive neck growth were found in the powders which were heated at 4°C/h and quenched from 650°C and 700°C (Figure 9). The morphologies of two as-calcined powders (0.58 and 6.5 mole % Bi_2O_3) and four sintered powders (0.58 and 6.5 mole % Bi_2O_3, quenched from 650°C and 700°C) are shown in Appendix B.

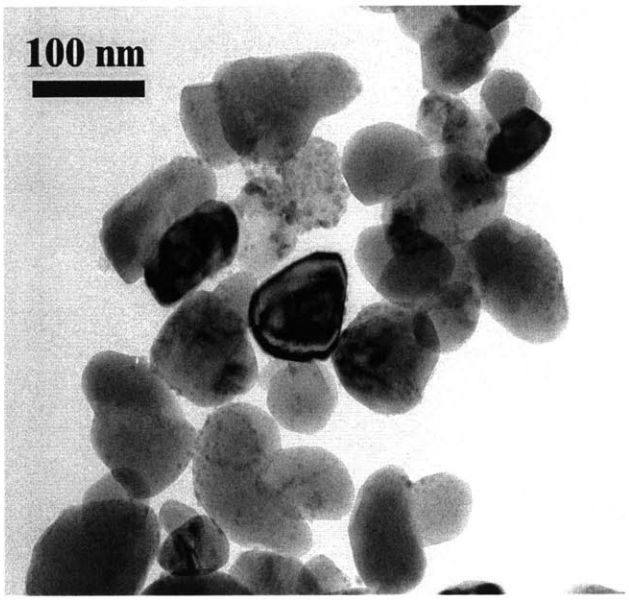

Figure 8 TEM micrograph of as-calcined ZnO + 0.58 mole % Bi_2O_3 powder.

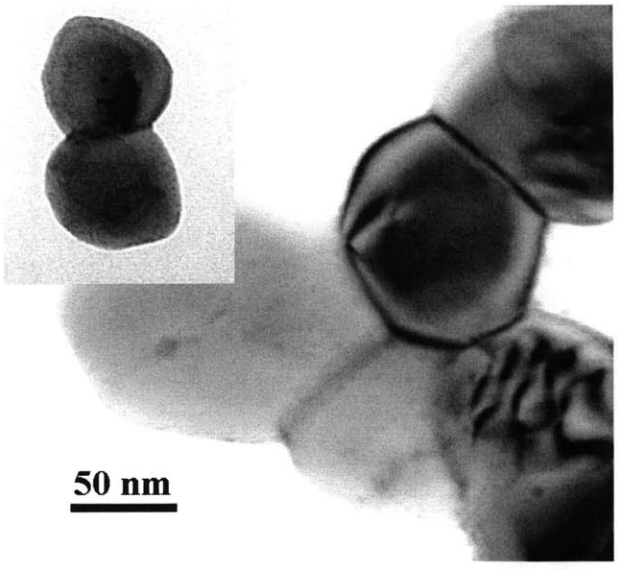

Figure 9 TEM micrographs of ZnO + 0.58 mole % Bi_2O_3 powder, sintered at 4°C/h and air-quenched from 700°C. The inset shows a pair of particles exhibiting extensive neck growth and suggesting center-to-center approach.

Table 1 lists the particle sizes of the ZnO + 0.58 mole % Bi_2O_3 powder before and after firing. The average particle size grows by a factor of approximately 2 and 3 respectively for heating to 650°C and 700°C for the powder sintered at 4°C/hour, indicating significant particle coarsening below the bulk eutectic temperature.

Table 1. Particle size statistics for ZnO + 0.58 mole % Bi_2O_3 powder, as-calcined and sintered. The sintered powders were heated at 4°C/hour, and air-quenched from 650°C and 700°C respectively.

Powder	As-Calcined	Quenched from 650°C	Quenched from 700°C
Average Size	72nm	177nm	221nm
Standard Deviation	27nm	86nm	121nm

3.3 Bismuth Distribution and Intergranular Amorphous Films

In three powders sintered at 4°C/h: (1) ZnO + 0.58 mole % Bi_2O_3, air-quenched from 700°C; (2) ZnO + 6.5 mole % Bi_2O_3, air-quenched from 650°C; and (3) ZnO + 6.5 mole % Bi_2O_3, air-quenched from 700°C, the bismuth and zinc distributions were mapped using STEM. In all of these powders, strong bismuth segregation was observed at grain boundaries, as shown in Appendix C. One typical example is shown in Figure 10.

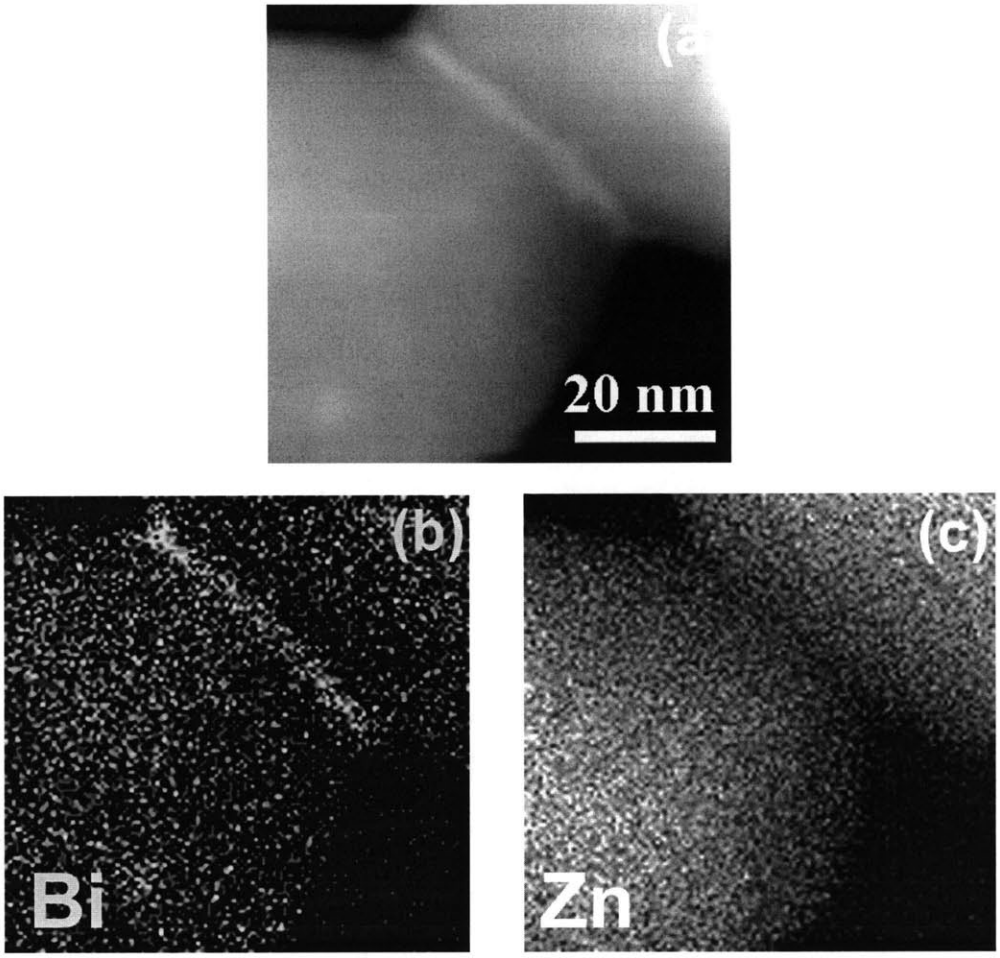

Figure 10 STEM (a) dark field image, (b) bismuth map, and (c) zinc map of sintered ZnO + 0.58 mole % Bi_2O_3 powder heated at 4°C/h and air-quenched from 700°C.

Because the powder diameter ranges from 100 nm to 300 nm, which is relatively thick for 200 kV microscopy, HREM was conducted primarily at the boundaries between smaller particles. Intergranular amorphous films were observed at all boundaries that could be oriented with the boundary plane parallel to the incident electron beam. Figure 11 shows a typical boundary, with an intergranular film approximately 0.8 nm thick.

These films are similar to those previously observed at solid-state equilibrium in sintered polycrystals [30].

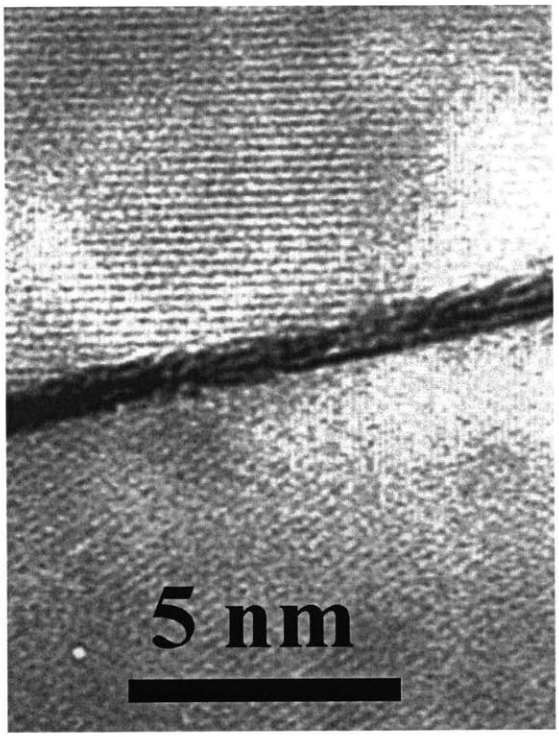

Figure 11 HREM image of an intergranular amorphous film in ZnO + 0.58 mole % Bi_2O_3 powder sintered at 4°C/h and air-quenched from 700°C.

It was further observed that the amorphous phase forms wetting menisci at sinter-necks (Figure 12), with a small contact angle at both the surfaces and grain boundary. A crystalline bismuth oxide was observed at several grain junctions (Figure 13). Unlike the amorphous phase, this crystalline secondary phase does not form a wetting configuration. We presume this phase to be that seen by X-ray diffraction. Since no ion milling was involved in preparing these specimens, we believe these secondary phase distributions are representative of those present during sintering.

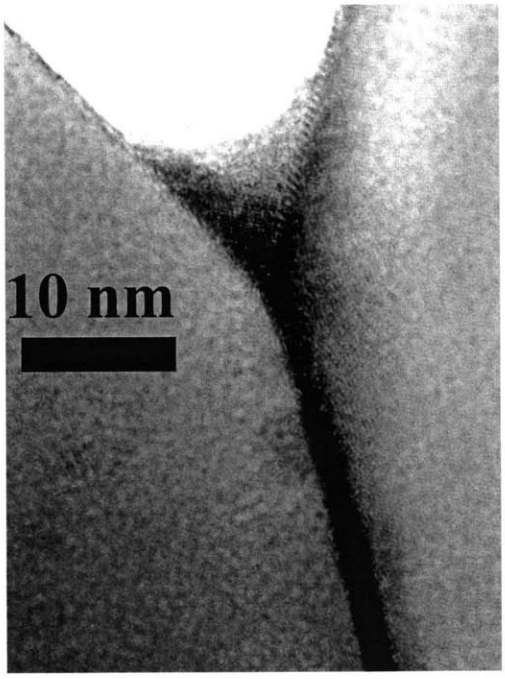

Figure 12 A typical wetting amorphous meniscus in ZnO + 6.5 mole % Bi_2O_3 powder (isothermally sintered at 650°C for 45 hours, and air-quenched).

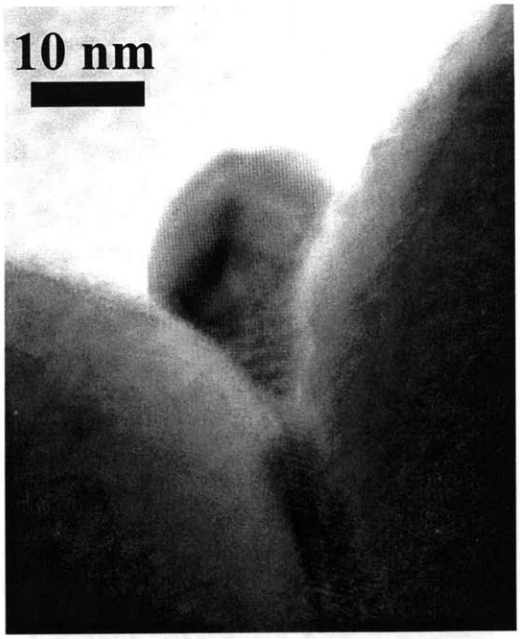

Figure 13 A non-wetting crystalline phase in ZnO + 0.58 mole % Bi_2O_3 powder (isothermally sintered at 700°C for 10 hours, and air-quenched).

3.4 Surface Amorphous Films

In a few instances, amorphous films of ~1 nm thickness were also observed at free surfaces of sintered ZnO powders. One such surface viewed edge-on is shown in Figure 14. Statistically, only a small fraction of surfaces are covered with amorphous films.

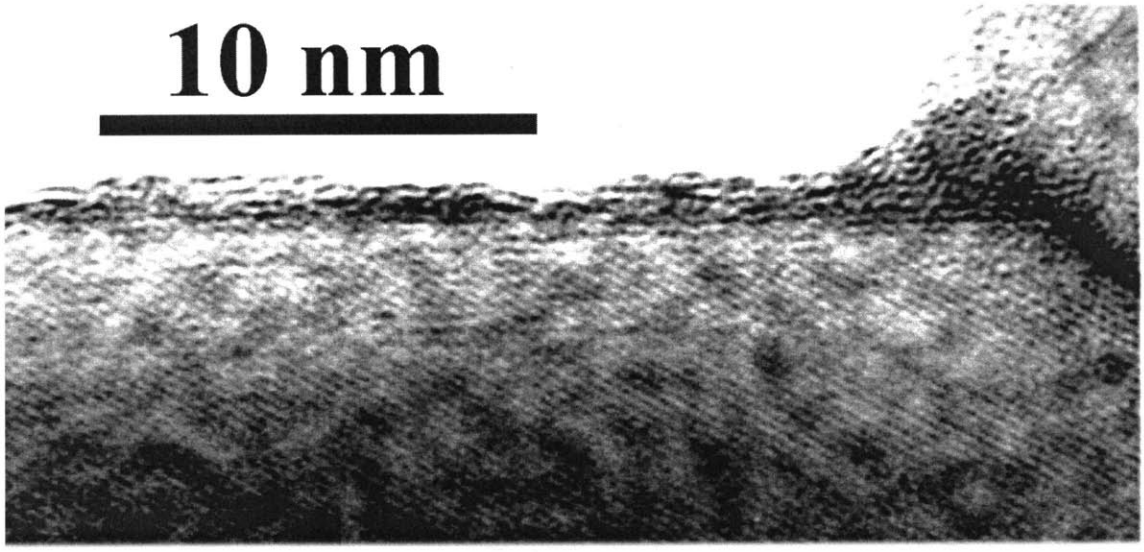

Figure 14 A surface amorphous film in ZnO + 0.58 mole % Bi_2O_3 powder sintered at 4°C/h, and air-quenched from 700°C.

4. Discussion

This study shows that an intergranular amorphous phase that satisfies the prerequisites for being an "activator" phase forms concurrently with the onset of solid-state activated sintering. This amorphous phase has a high solubility for the ZnO primary phase, spontaneously forms continuous films along grain boundaries, and has an increased diffusion coefficient for at least oxygen [37]. Although the zinc grain

boundary diffusion coefficient has not been measured, it is reasonable to expect that it is also increased in the intergranular film. Rapid mass transport of ZnO through the intergranular films is therefore concluded to be the mechanism of solid-state sintering in this system. Moreover, the amorphous phase forms wetting menisci at sinter-necks, indicating that it can provide a capillary pressure driving force for solid-state sintering.

Compared with previous explanations of activated sintering, this model is unique in that the "activator" is an amorphous phase that forms well below the eutectic temperature, and only at interfaces. This phase does not appear in the bulk phase diagram. Previous work has shown [30] that the intergranular amorphous films in Bi_2O_3-doped ZnO form at thermodynamic equilibrium and below the eutectic temperature. The present experiments further support the existence of sub-eutectic amorphous films, and are significant in that the samples have not been ion-thinned, therefore removing the possibility of preparation artifacts. The sub-eutectic intergranular amorphous film can be stable if the increased volume free energy of amorphization is compensated by reduction of the total interfacial energy compared with a ZnO-ZnO grain boundary. In addition to the reduction in interfacial energy upon replacing the crystalline grain boundary with two glass-crystal interfaces, it is expected that the van der Waals interaction and short-range ordering will contribute to the total energy of the film [23-24]. The appearance of an "equilibrium thickness" for the solid-state amorphous film suggests existence of a local minimum in the total interaction energy.

The previous studies [25, 30] have also shown that the composition of the intergranular films at 700°C is about 2.3 ZnO : 1 Bi_2O_3, which is distinctly zinc rich

compared to the eutectic liquid (15% ZnO : 85% Bi_2O_3). For this composition, the equilibrium liquidus temperature is ~1600°C [21-22]. Given the magnitude of the undercooling, we infer that the intergranular films are glassy rather than sub-eutectic metastable liquid at the present sintering temperatures of 650-700°C. The intergranular phase also does not appear to be a ternary liquid caused by the presence of an impurity (e. g., PbO) that could significantly lower the solidus temperature. STEM analysis has not revealed the presence of any detectable impurities in the amorphous phase.

It is not surprising that at low concentrations the activated sintering behavior is affected by the bismuth oxide content. The formation of intergranular films requires bismuth transport to the grain boundary region. Beacuse the solid solubility of bismuth in ZnO is limited, (<0.06 mole % Bi_2O_3 in ZnO at the eutectic temperature [39]) we assume that the bismuth oxide is transported by the evaporation - condensation or surface diffusion. When the overall bismuth content is low and the bismuth distribution is not completely homogenous, film formation may be inhibited. Other authors have also observed that activated sintering does not occur in lightly bismuth-doped samples, and the sintering behavior is always powder specific [16, 17]. Larger shrinkage has been observed at higher heating rates in other studies [17, 19], but generally in samples of higher bismuth contents [19], or in multiply-doped samples [17].

In the high bismuth content sample (6.5 mole % Bi_2O_3), the densification below 650°C is significantly higher than that in low bismuth-content samples (Figure 2). This is possibly due to increased particle re-arrangement, given the excess of secondary phase. However, in this sample as well as the one containing 0.58 mole % Bi_2O_3, intensive

activated sintering begins at about 700°C, which indicates that the process is similar in both.

The surface amorphous films, which also appear to be of "equilibrium thickness," are most likely the free-surface counterpart of intergranular amorphous films of equilibrium thickness. These have now been observed at grain boundaries in numerous systems [23-24, 27-29], as well as at heterophase interfaces [26, 29]. Since in our samples only a small fraction of the ZnO surface is covered by surface films, they probably do not contribute significantly to activated sintering.

It is possible that intergranular films of a similar character are responsible for activated sintering in other systems. In nickel- and palladium-activated sintering of tungsten, several studies [8, 40, 41] concluded that diffusion in the interfacial phase is the rate-limiting step. This would suggest that the sintering rate would increase for a thicker layer of activator phase. However, experiments have deduced that the optimum coating layer thickness is about one nanometer, above which the shrinkage rate remains steady [9] or even slightly decreases [8]. Although further study is necessary to clarify to nature of the activator phase in refractory metals, it is possible that any excess solute above that necessary to form an equilibrium-thickness film forms discrete secondary phase that does not promote sintering.

5. Conclusion

Small additions of uniformly distributed Bi_2O_3 can greatly enhance the sintering of ZnO powders below the bulk eutectic temperature. Pre-eutectic densification, neck

growth and particle coarsening have been observed to occur in the solid state. Bi-enriched amorphous films of ~1 nanometer thickness form at grain boundaries during solid-state activated sintering. Consequently, accelerated mass transport through these sub-eutectic intergranular amorphous films appears to be responsible for activated sintering in this system. Moreover, the amorphous phase is found to form wetting menisci at particle contacts providing a capillary pressure driving force for solid-state sintering.

Appendix A:

Morphologies of As-Precipitated (Pre-Calcined) Powders

The following pages contain the TEM images of as-precipitated (pre-calcined) powders:

(1) ZnO + 0.23 mole % Bi_2O_3.

(2) ZnO + 0.58 mole % Bi_2O_3.

(3) ZnO + 6.5 mole % Bi_2O_3.

The powders were provided by Dr. J. –R. Lee.

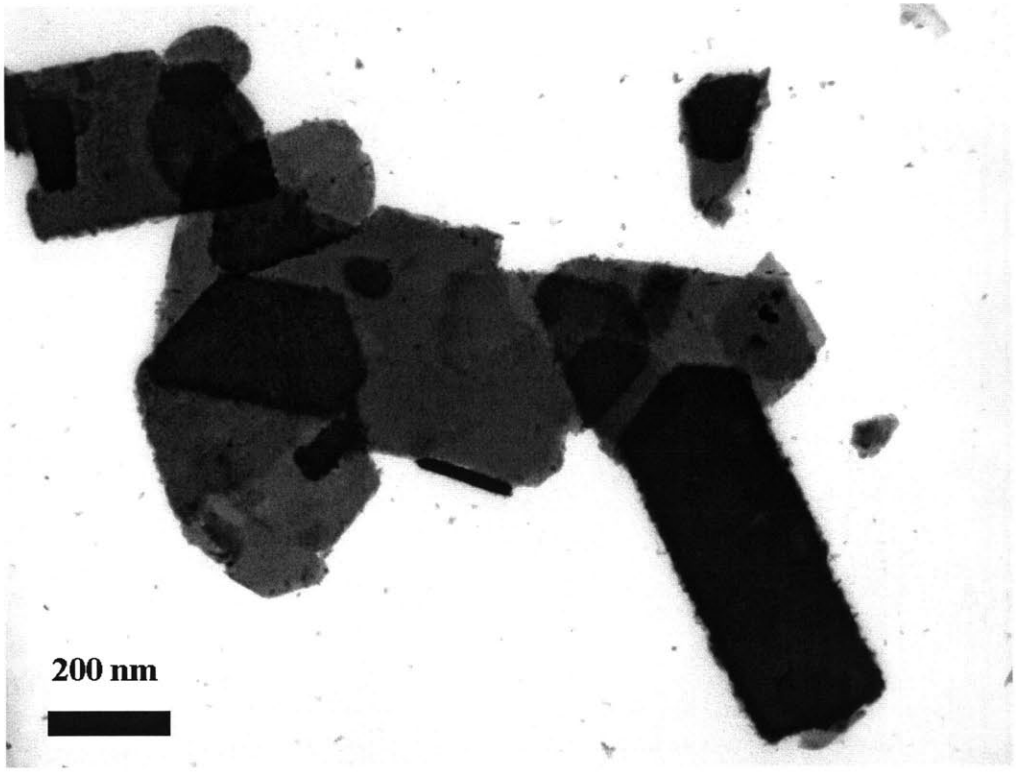

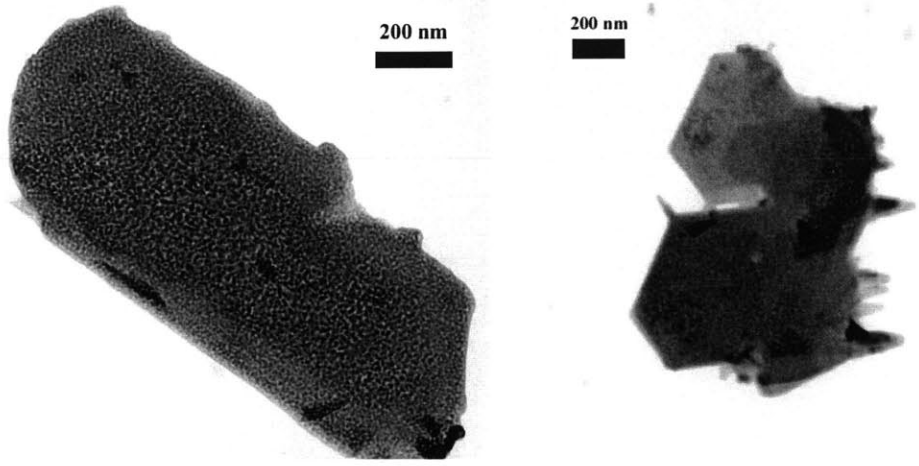

ZnO + 0.23 mole % Bi_2O_3, as-precipitated.

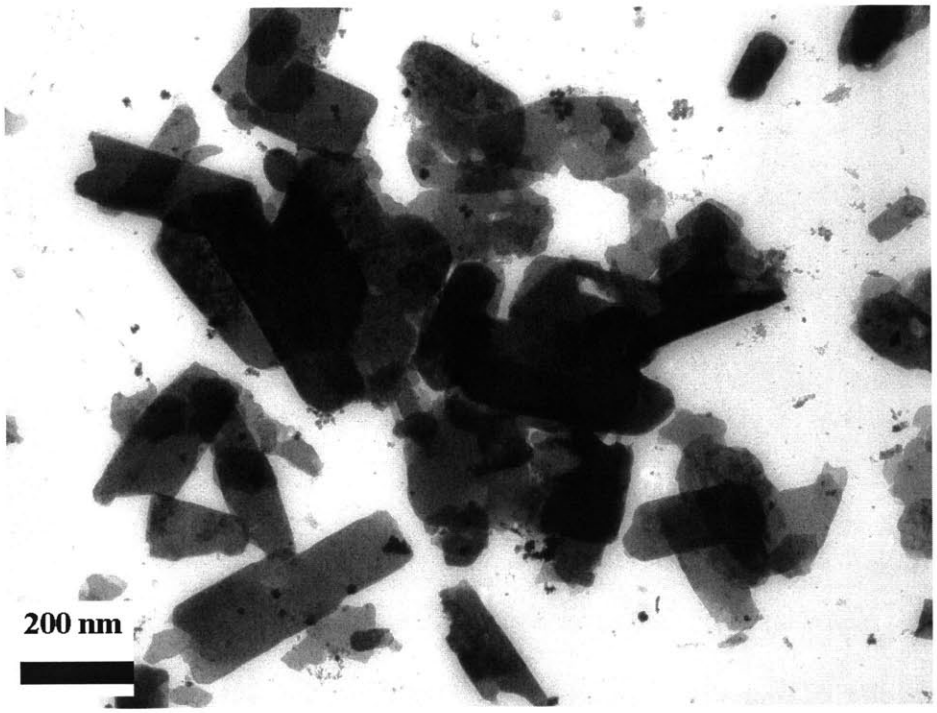

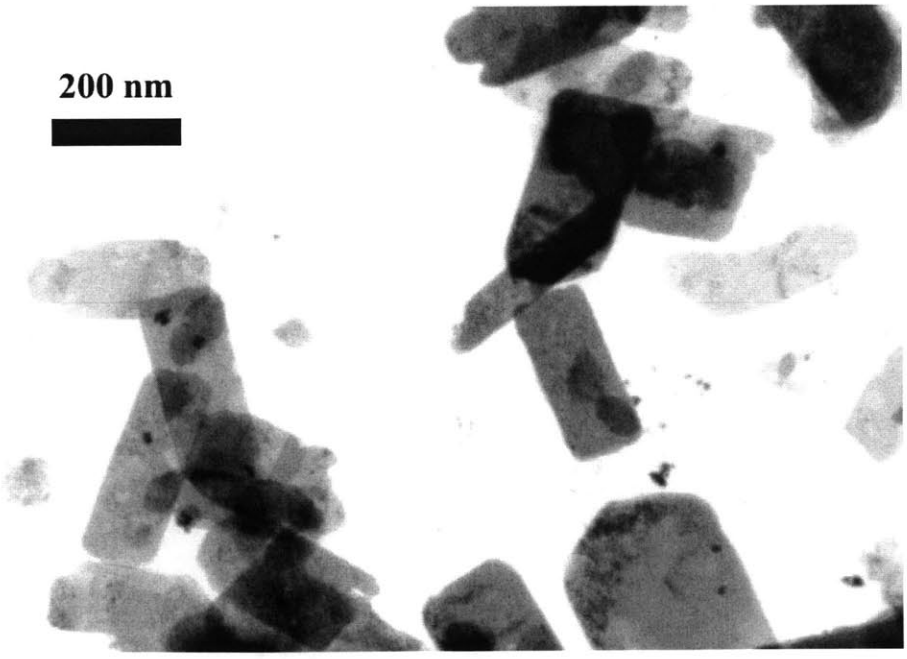

ZnO + 0.58 mole % Bi_2O_3, as-precipitated.

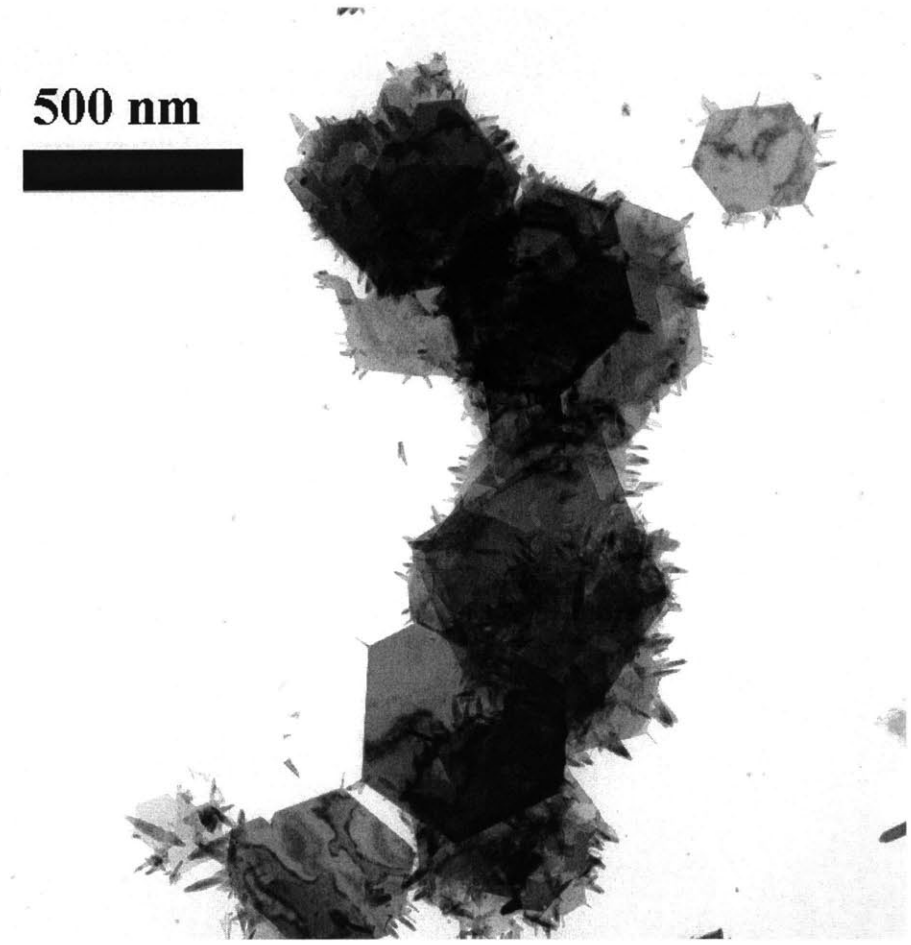

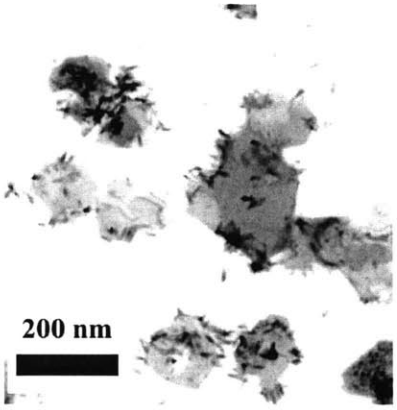

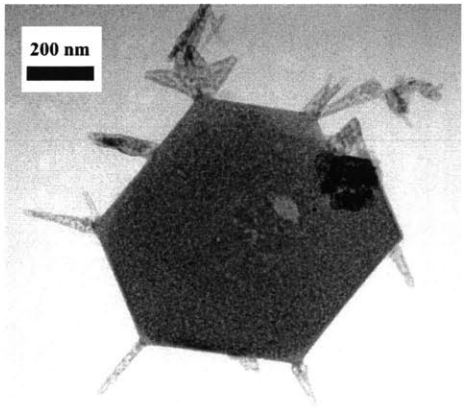

ZnO + 6.5 mole % Bi_2O_3, as-precipitated.

Appendix B:

Morphologies of As-Calcined and Sintered Powders

The following pages contain the TEM images of as-calcined and sintered powders:

(1) ZnO + 0.58 mole % Bi_2O_3, as-calcined (550°C, 2h).

(2) ZnO + 0.58 mole % Bi_2O_3, sintered at 4°C/h, air-quenched from 650°C.

(3) ZnO + 0.58 mole % Bi_2O_3, sintered at 4°C/h, air-quenched from 700°C.

(4) ZnO + 6.5 mole % Bi_2O_3, as-calcined (550°C, 2h).

(5) ZnO + 6.5 mole % Bi_2O_3, sintered at 4°C/h, air-quenched from 650°C.

(6) ZnO + 6.5 mole % Bi_2O_3, sintered at 4°C/h, air-quenched from 700°C.

Classical sintered powder morphologies with extensive neck growth were found in all sintered powders

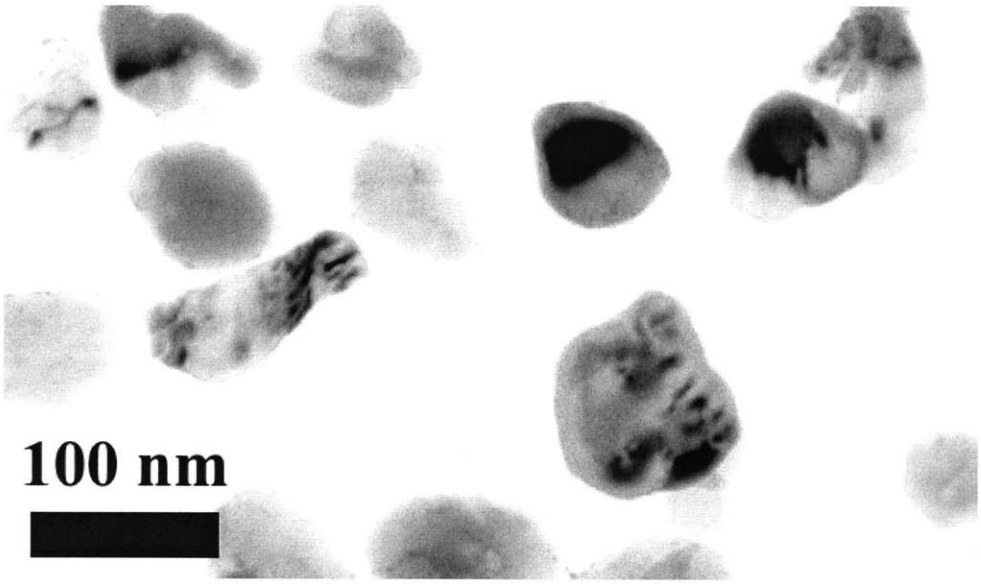

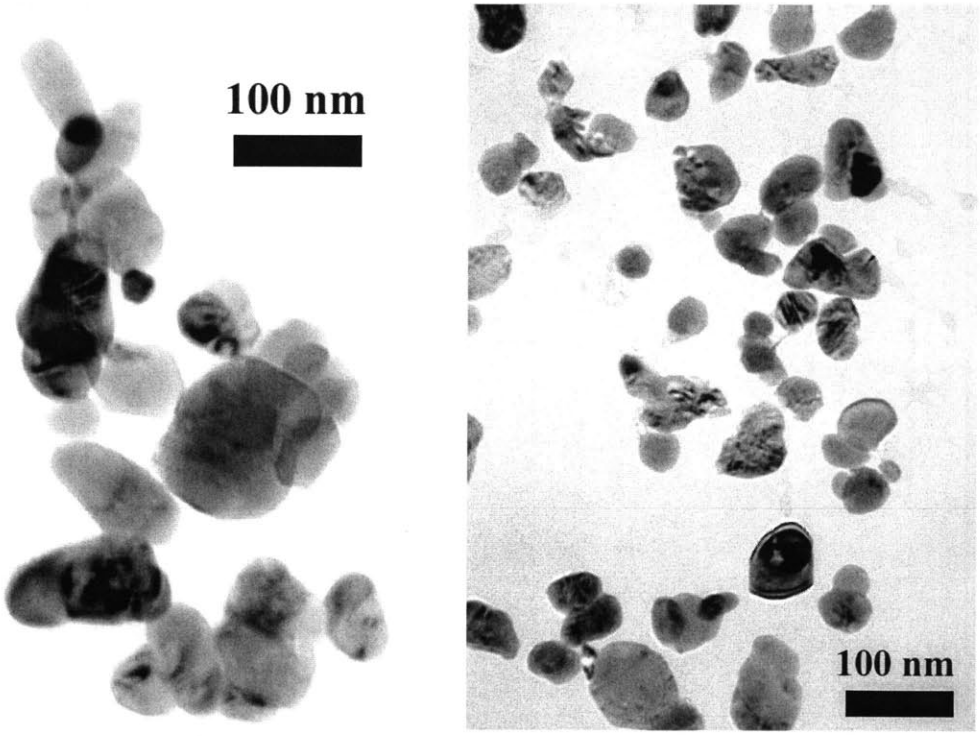

$ZnO + 0.58$ mole % Bi_2O_3,
as-calcined (500°C, 2h).

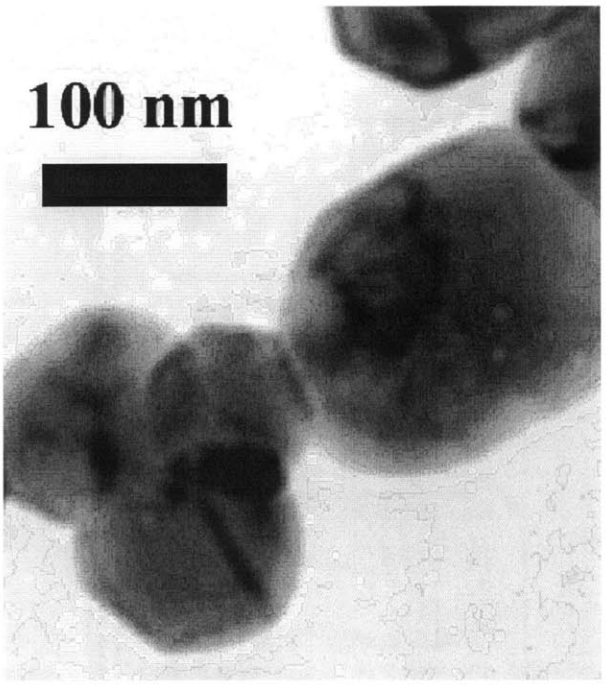

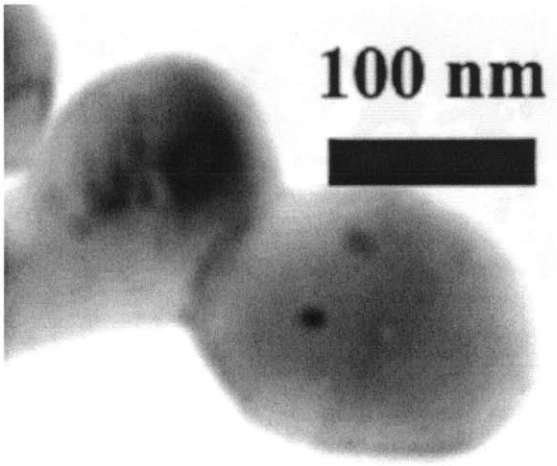

ZnO + 0.58 mole % Bi_2O_3,
sintered at 4°C/h, quenched from 650°C.

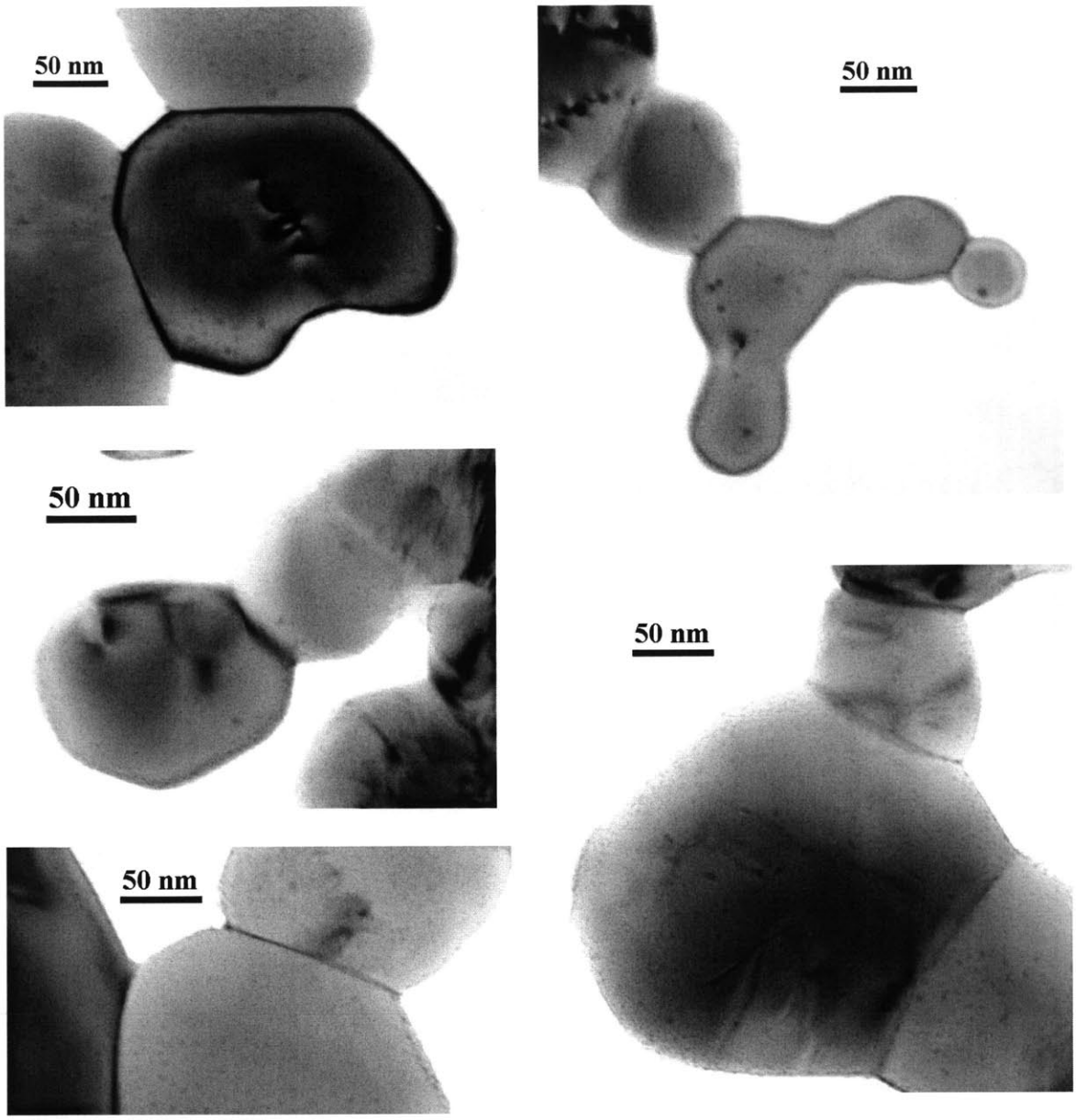

ZnO + 0.58 mole % Bi_2O_3,
sintered at 4°C/h, quenched from 700°C.

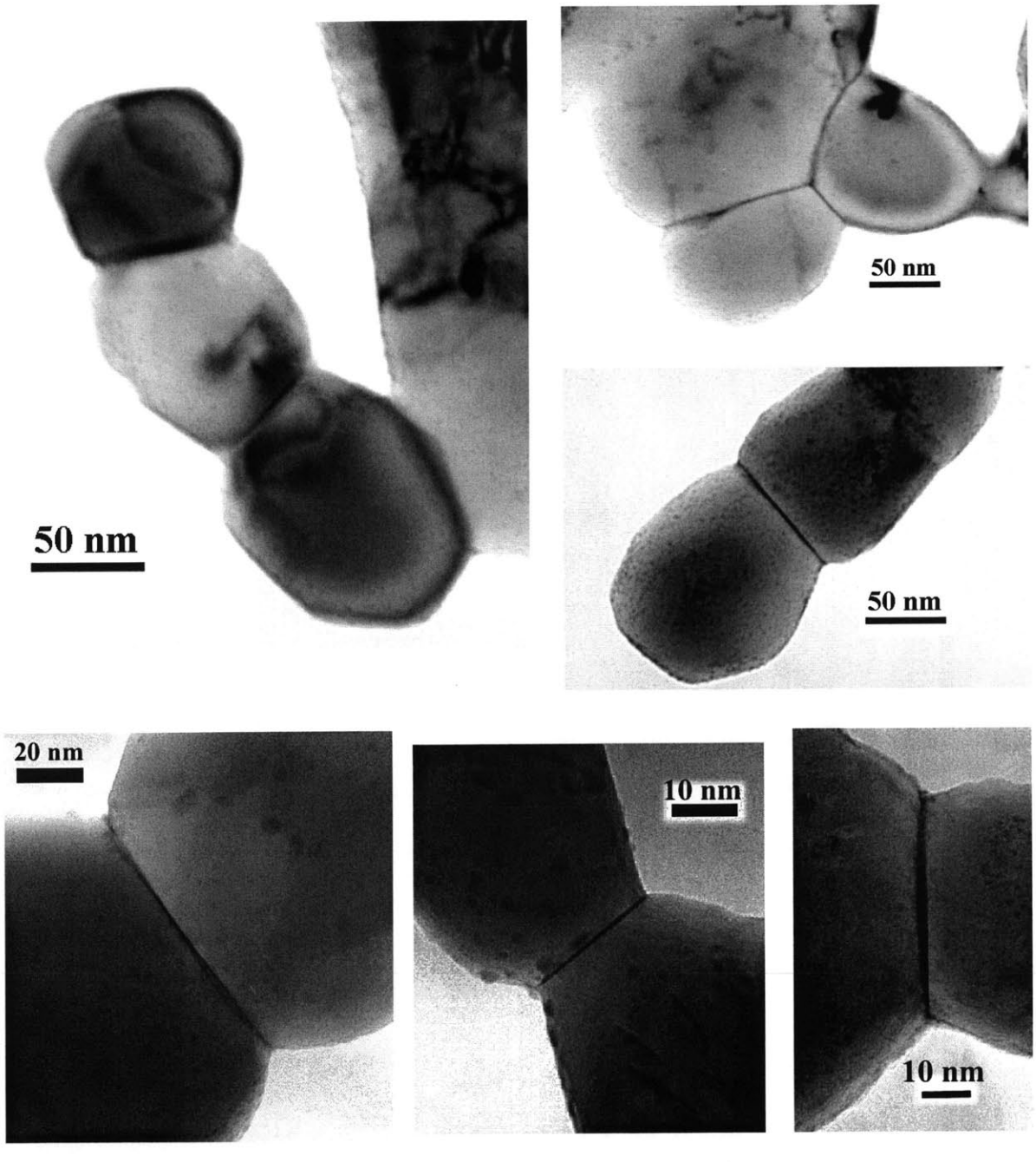

ZnO + 0.58 mole % Bi_2O_3,
sintered at 4°C/h, quenched from 700°C.

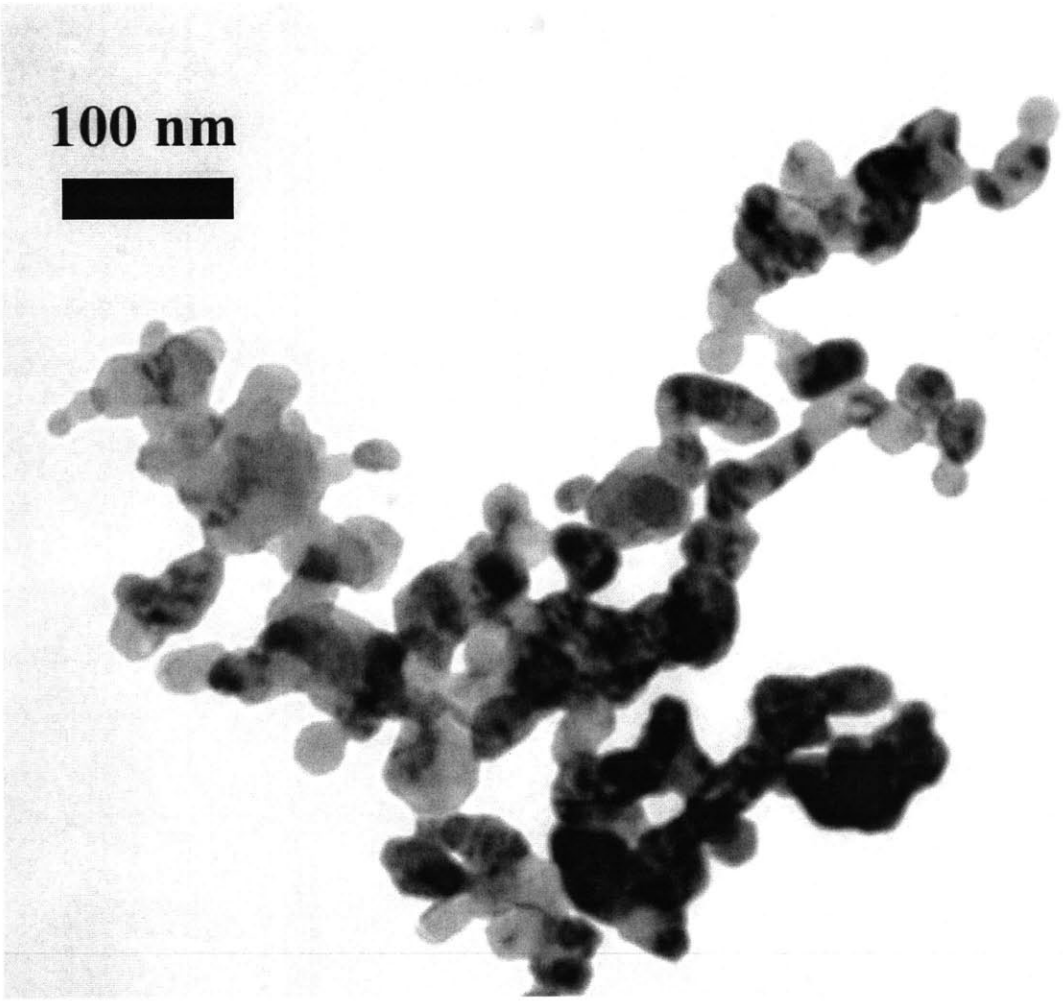

ZnO + 6.5 mole % Bi_2O_3,
as-calcined (500°C, 2h).

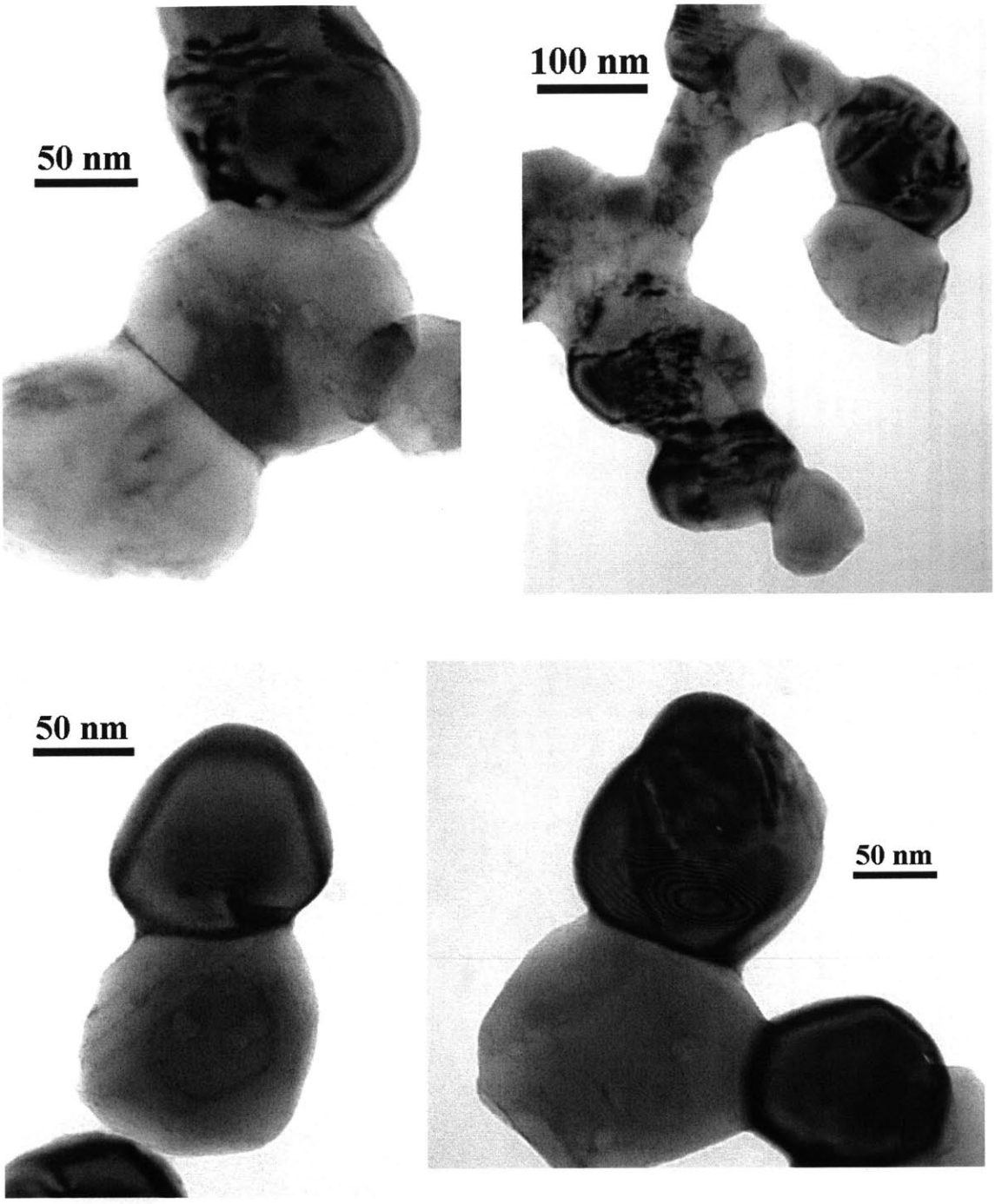

ZnO + 6.5 mole % Bi_2O_3,
sintered at 4°C/h, quenched from 650°C.

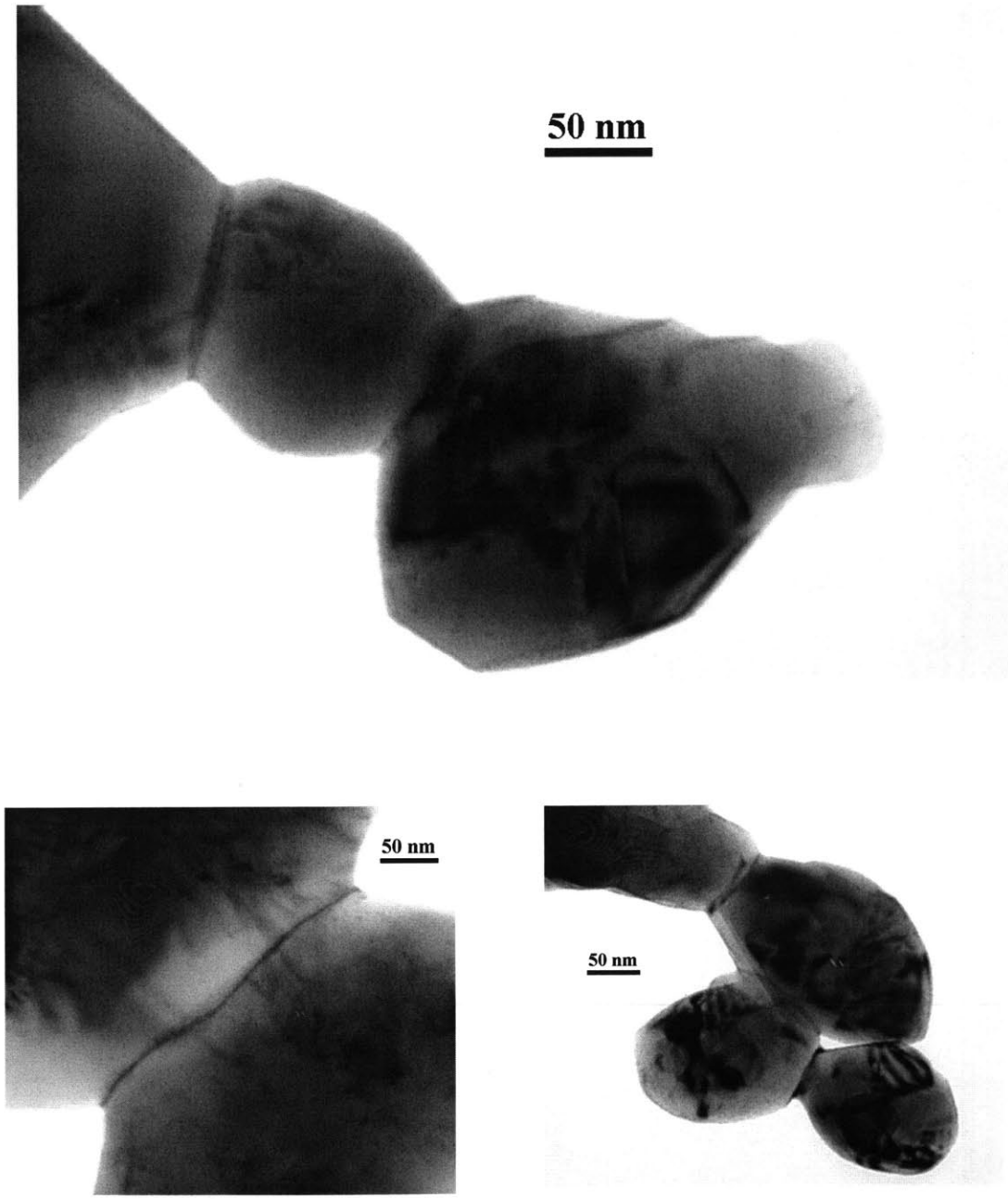

ZnO + 6.5 mole % Bi_2O_3,
sintered at 4°C/h, quenched from 700°C.

Appendix C:

STEM Maps of Sintered Powders

The following pages contain the STEM images, bismuth and zinc maps of three powders sintered at 4°C/h:

(1) ZnO + 0.58 mole % Bi_2O_3, air-quenched from 700°C.

(2) ZnO + 6.5 mole % Bi_2O_3, air-quenched from 650°C.

(3) ZnO + 6.5 mole % Bi_2O_3, air-quenched from 700°C.

Strong bismuth segregation was observed at all grain boundaries.

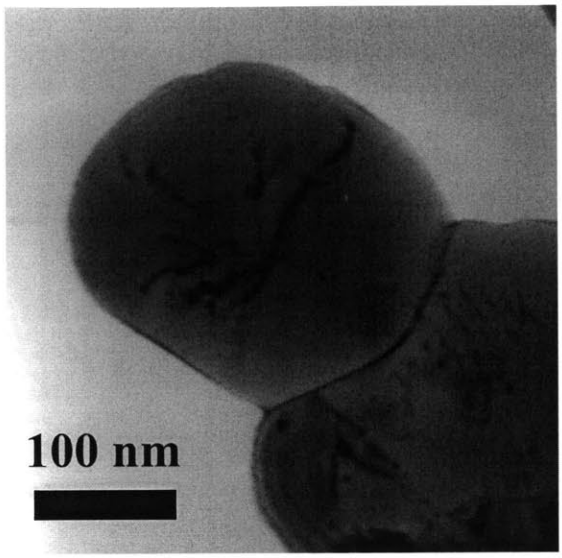

STEM Bright Field Image

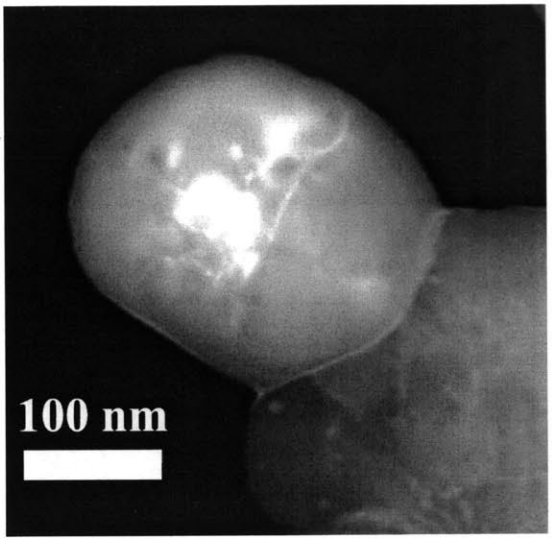

STEM Dark Field Image

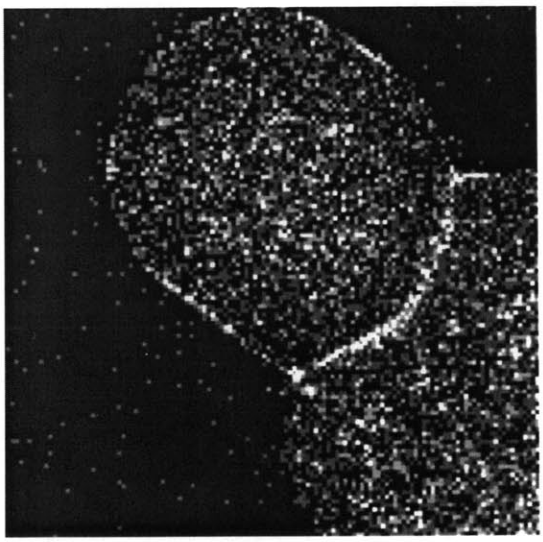

Bi Map

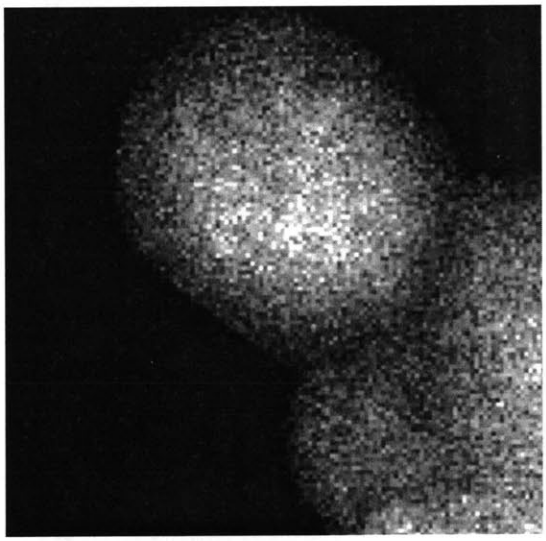

Zn Map

$ZnO + 0.58$ mole % Bi_2O_3,
sintered at 4°C/h, quenched from 700°C.

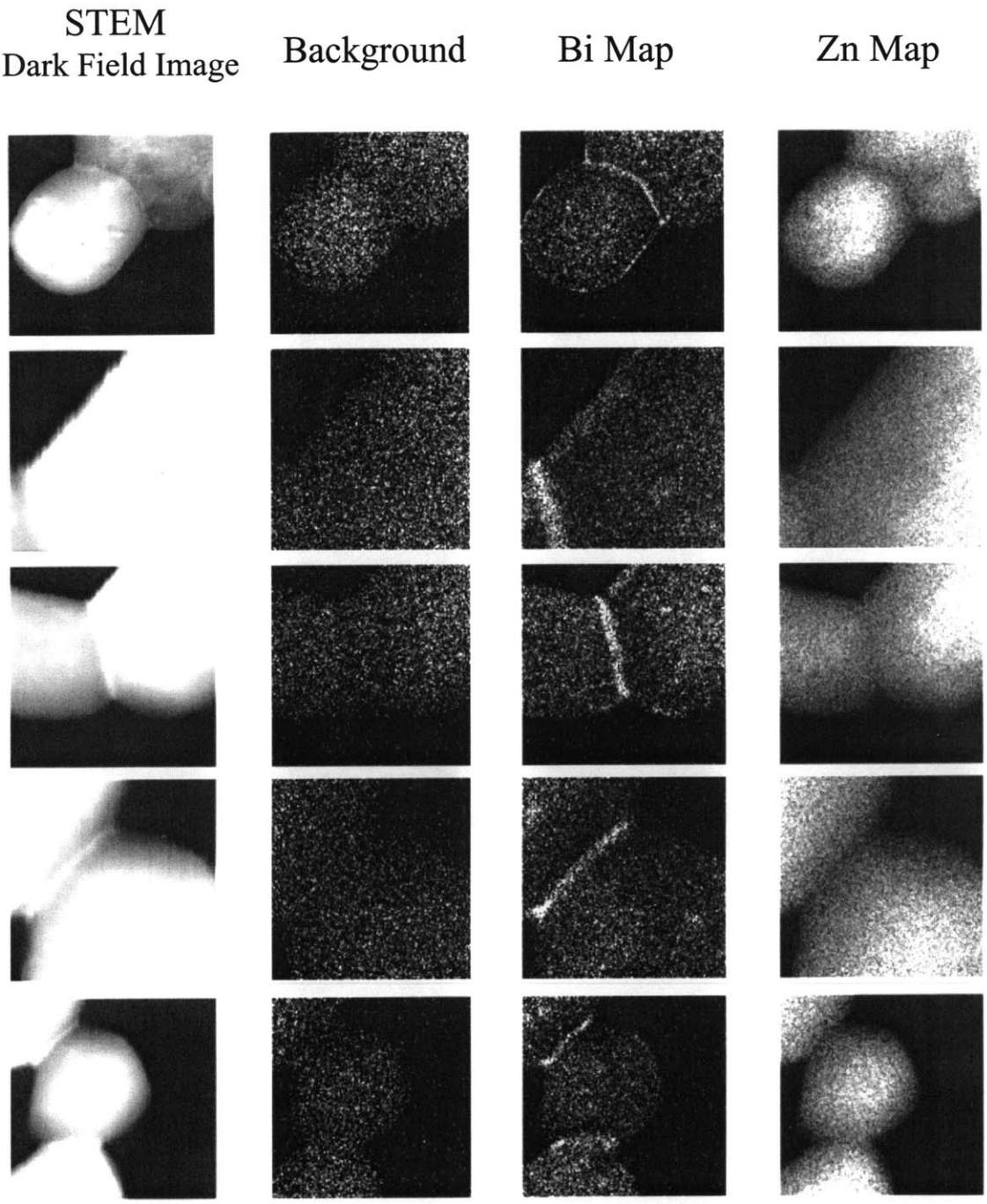

$ZnO + 0.58$ mole % Bi_2O_3,
sintered at 4°C/h, quenched from 700°C.

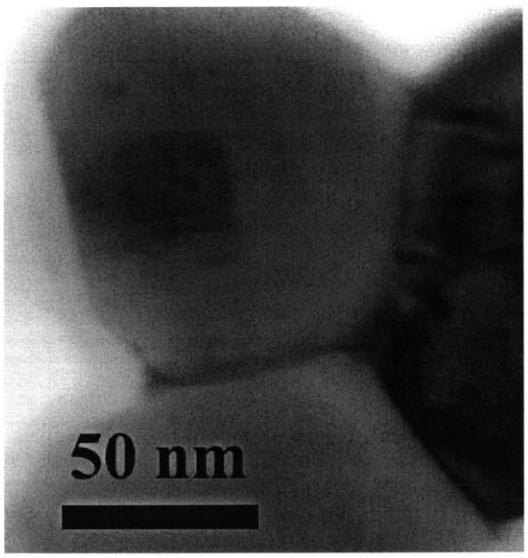

STEM Bright Field Image

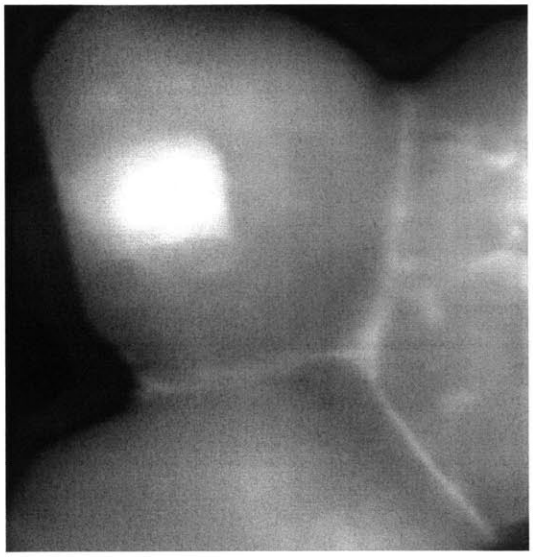

STEM Dark Field Image

Bi Map

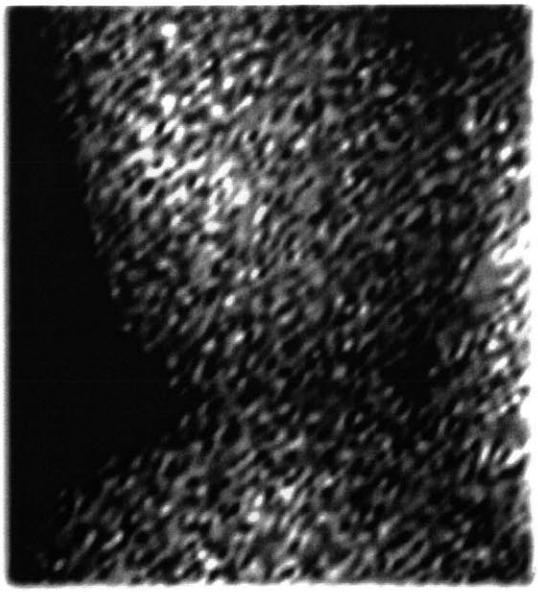

Zn Map

$ZnO + 6.5$ mole % Bi_2O_3,
sintered at 4°C/h, quenched from 650°C.

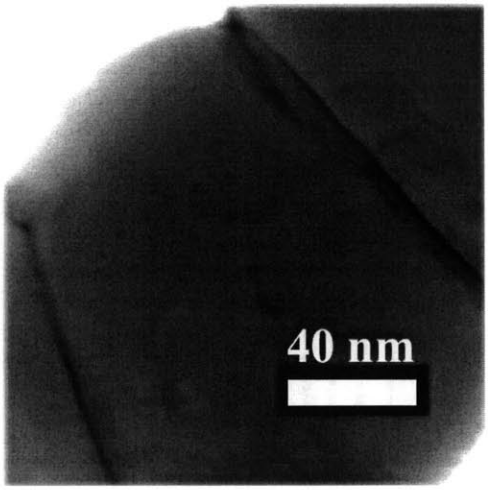

STEM Bright Field Image

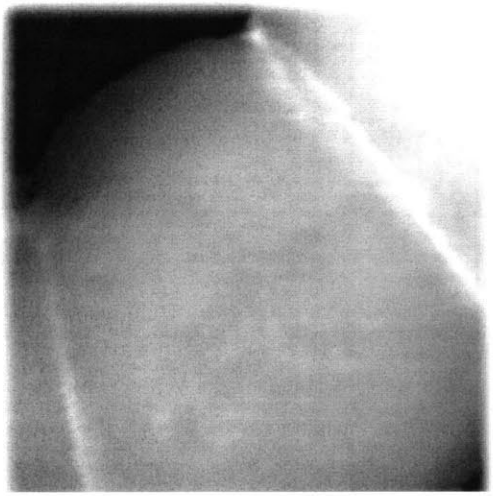

STEM Dark Field Image

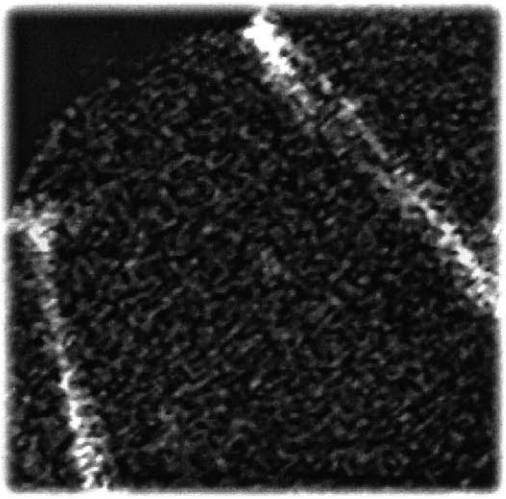

Bi Map

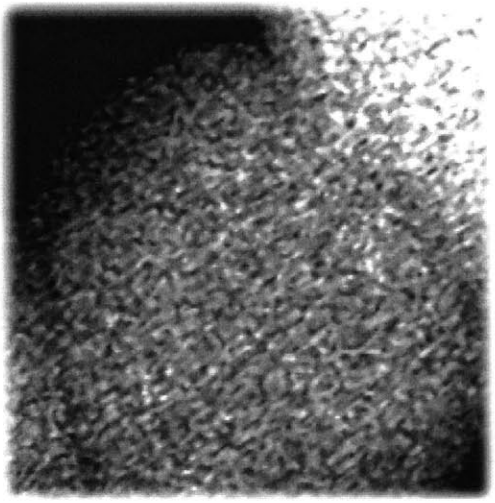

Zn Map

$ZnO + 6.5$ mole % Bi_2O_3,
sintered at 4°C/h, quenched from 700°C.

Bibliography

1. W. D. Kingery, "Densification during Sintering in the Presence of a Liquid Phase. I. Theory," *J. Appl. Phys.*, **30**, 301-10 (1959)
2. J. H. Brophy, L. A. Shepard, and J. Wulff, "The Nickel-Activated Sintering of Tungsten," *Powder Metallurgy*, ed. W. Leszynski, p.113-35, Interscience, New York (1961)
3. R. Watanabe, K. Taguchi, and Y. Masuda, "Activated Sintering of Chromium with Palladium Addition," *Sci. Sintering*, **15** [2], 73-80 (1983)
4. Y. Mil'man, M. M. Ristic, I. V. Gridneva, D. V. Lotsko, I. Kristanovich, and V. A. Goncharuk, "Structure and Hardness of Sintered Mo-Ni Alloys," *Sov. Powder Metall. Met. Ceram.*, **V26**, 144-48 (1987)
5. G. Li, "Activated Sintering of MgO-CaO Series," *Sci. Sintering*, **19** [3], 167-78, (1987)
6. E. C. Skaar, "Activated Sintering in Calcium Fluoride, Sodium Fluride System," Ph.D. thesis, M.I.T., Cambridge, MA, 1977
7. P. H. Duvigneaud, and D. Reinhard, "Activated Sintering of Tin Dioxide," *Science of Ceramics*, **V12**, p.287-92 (1984)
8. I. J. Toth, and N. A. Lockington, "The Kinetics of Metallic Activation Sintering of Tungsten," *J. Less-Common Metals*, **12**, 353-65 (1967)
9. R. M. German, "Diffusional Activated Sintering – Densification, Microstructure and Mechanical Properties," *Prog. Powder Met.*, **39**, 243-54 (1984)
10. J. L. Johnson, and R. M. German, "Theoretical Modeling of Densification During Activated Solid-State Sintering," *Metall. Met. Trans.* **27A**, 441-50 (1996)
11. R. M. German, "The Identification of Enhanced Sintering Systems Through Phase Diagrams," *Modern Development in Powder Metallurgy*, **15**, 253-73 (1985)
12. P. E. Zovas, R. M. German, K. S. Hwang, and C. J. Li, "Activated and Liquid-Phase Sintering – Progress and Problems," *J. Met.*, **35** [1], 28-32, (1983)
13. L. M. Levinson, and H. R. Philipp, "Application and Characterization of ZnO Varistors," *Ceramic Materials for Electronics, Processing, Properties, and Applications,* 2nd Edition, ed. R. C. Buchanan, p.349-77, Marcel Dekker, Inc. (1991)
14. T. K. Gupta, "Application of Zinc Oxide Varistor," *J. Am. Ceram. Soc.*, **73** [7], 1817-40 (1990)
15. D. Dey, and R. C. Bradt, "Grain Growth of ZnO During Bi_2O_3 Liquid-Phase Sintering," *J. Am. Ceram. Soc.*, **75** [9], 2529-34 (1992)
16. E. P. Rothman, "Activated Sintering of Bismuth-Doped Zinc Oxide Ceramics," M. S. thesis, M.I.T., Cambridge, MA, June 1982
17. M. N. Rahaman, L. C. De Jonghe, J. A. Voigt, and B. A. Tuttle, "Low-Temperature Sintering of Zinc Oxide Varistors," *J. Mater. Sci.*, **25**, 737-42 (1990)
18. M. Ghirlanda and L.C. De Jonghe, "Sintering of Doped ZnO Powders: Relationship between Grain Growth and Sintering Stress," *Mater. Sci. Forum*, **94-96**, 855-64 (1992)

19. A. Peigney and A. Rousset, "Phase Transformation and Melting Effects During the Sintering of Bismuth-Doped Zinc Oxide Powders," *J. Am. Ceram. Soc.*, **79**(8) 2113-26 (1996)
20. J. Kim, T. Kimura, and T. Yamaguchi, "Effect of Bismuth Oxide Content on the Sintering of Zinc Oxide," *J. Am. Ceram. Soc.*, **72** [8], 1541-44 (1989)
21. G. M. Safronov, V. N. Batog, T. V. Stepanyuk, and P. M. Fedorov, "Equilibrium Diagram of Bismuth Oxide - Zinc Oxide," *Russ. J. Inorg. Chem.* **16** [3], 460-61 (1971)
22. Powder Diffraction File, card No.41-0253.
23. D. R. Clarke, "On the Equilibrium Thickness of Intergranular Glass Phases In Ceramic Materials," *J. Am. Ceram. Soc.*, **70** [1], 15-22 (1987)
24. H. D. Ackler, "Thermodynamic Calculations and Model Experiments on Thin Intergranular Amorphous Films in Ceramics," Ph.D. thesis, MIT, Cambridge, MA, February, 1997
25. Y, -M. Chiang, H. Wang, J. –R. Lee, "HRTEM and STEM of Intergranular Films at Zinc Oxide Varistor Grain Boundaries," *J. Microscopy*, **191** [3], 275-85 (1998)
26. H.-J. Kleebe, M. J. Hoffman, and M. Rühle, "Influence of Secondary Phase Chemistry on Grain Boundary Film Thickness in Silicon Nitride," *Z. Metallkd.*, **83** [8], 610-17 (1992)
27. H. -J. Kleebe, M. K. Cinibulk, R. M. Cannon and M. Rühle, "Statistical Analysis of the Intergranular Film Thickness in Silicon Nitride Ceramics," *J. Am. Ceram. Soc.*, **76** [8], 1969-77 (1993)
28. Y. -M. Chiang, L. A. Silverman, R. H. French, and R. M. Cannon, "Thin Glass Film Between Ultrafine Conductor Particles in Thick-film Resistors," *J. Am. Ceram. Soc.*, **77** [5], 143-52 (1994)
29. H. D. Ackler and Y. -M. Chiang, "Model Experiment on Thermodynamic Stability of Retained Intergranular Amorphous Films," *J. Am. Ceram. Soc.*, **80** [7], 1893-96 (1997)
30. H. Wang and Y.-M. Chiang, "Thermodynamic Stability of Intergranular Amorphous Films in Bismuth-Doped Zinc Oxide," *J. Am. Ceram. Soc.* **81** [1], 89-96 (1998)
31. J. P. Gambino, W. D. Kingery, G. E. Pike, and H. R. Philipp, "Effect of Heat Treatments on the Wetting Behavior of Bismuth Rich Intergranular Phases in ZnO:Bi:Co varistors," *J. Am. Ceram. Soc.*, **72** [4], 642-45 (1989)
32. W. D. Kingery, J. B. Vander Sande and T. Mitamura, "A Scanning Transmission Electron Microscopy Investigation of Grain boundary Segregation in a ZnO-Bi_2O_3 Varistor," *J. Am. Ceram. Soc.*, **62** [3-4], 221-22 (1979)
33. J. -R. Lee, "Effect of Pressure and Thermal History on Grain Boundary Solute Coverage in ZnO-Bi_2O_3 and Relation to Varistor Properties," Ph.D. thesis, M.I.T., Cambridge, MA, June 1996
34. D. R. Clarke, "The Microstructural Location of the Intergranular Metal Oxide Phase in a Zinc Oxide Varistor," *J. Appl. Phys.*, **49** [4], 2407 (1978)
35. E. Olsson, L. K. L. Falk, and G. L. Dunlop, "The Microstructure of a ZnO Varistor Material," *J. Mater. Sci.*, **20** [11], 4091-98 (1985)

36. E. Olsson ,and G. L. Dunlop, " Characterization of Individual Interfacial Barriers in a ZnO Varistor Material," *J. Appl. Phys.*, **66** [8], 3666-75 (1989)
37. J. Claus, H. L. Tuller, J. -R. Lee, and Y. -M. Chiang, unpublished work.
38. H. A. Harwig, and A. G. Gerards, "The Polymorphism of Bismuth Sesquioxide," *Thermochimica Acta*, **28**, 121-31 (1979)
39. J. -R. Lee, Y. -M. Chiang, and G. Ceder, "Pressure-Thermodynamic Study of Grain Boundaries: Bi Segregation in ZnO," *Acta. Metall. Mater.*. **45**[3], 1247-57 (1997)
40. G. Flether, M. R. James, and J. R. Moon, "The Nickel Activated Sintering of Tungsten," *Scripta Met.* **5**, 105-108 (1971)
41. D. N. Lee, and S. H. Ahn, "Nickel Activated Model Sintering of Tungsten," *Sci. Sintering*, **11** [1], 43-45 (1979)